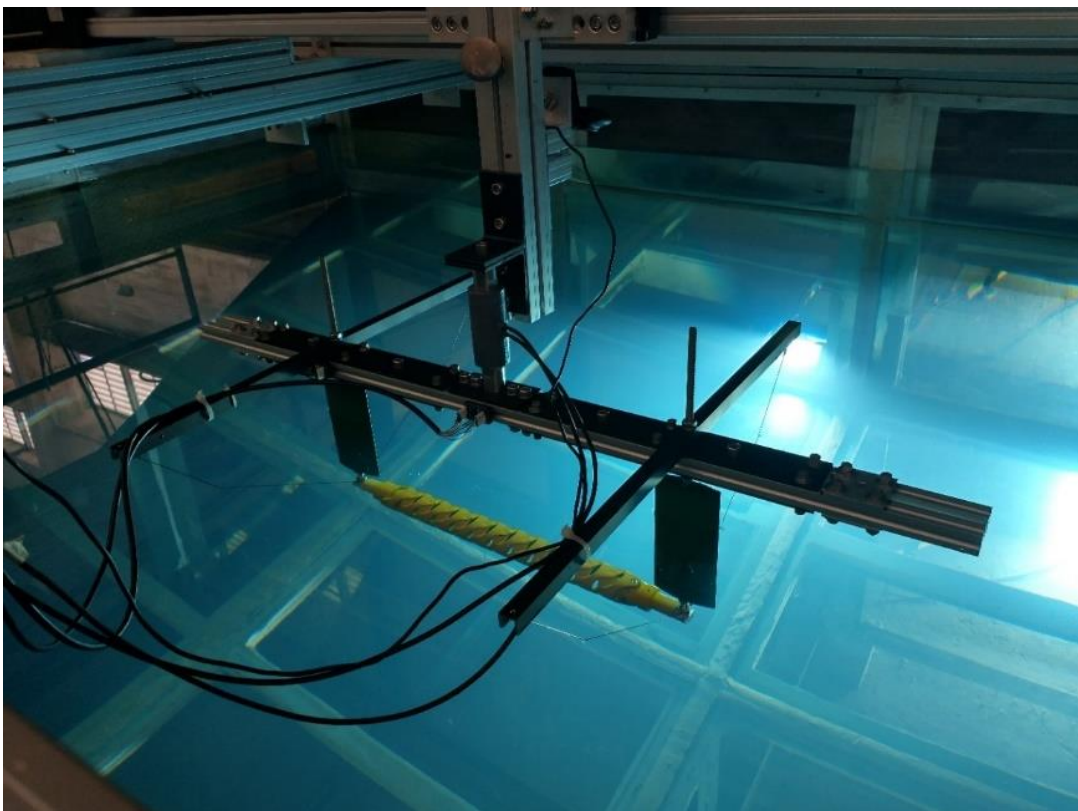


 Laboratório de Ondas e Correntes <small>COPPE/UFRJ</small>	Experimental Analysis Report	Issued by: Daniel Costa
		Approved by: Antonio Carlos Fernandes & Joel Sena Sales Junior
	SS7_21_02 - EAR_01_B	Issued: 2022/08/09

PROJECT	Code	SS7_21_02
	Title	Hydrodynamic Tests for Gimbal Joint Riser
	Client	Subsea7
	Effective date	2021
	Research manager	Daniel Costa
	Coordinators	Antonio Carlos Fernandes & Joel Sena Sales Junior



REPORT	Code	EAR_01
	Type	Experimental Analysis Report
	Author	Daniel Costa
	Title	Model Test Report of forced oscillation of Gimbal Joint Riser
	Revision	B
	Issued [aaaa/mm/dd]	2022/08/09

DOCUMENT HISTORY

DC = Daniel de Oliveira Costa – LOC

JS = Joel Sena Sales Junior – LOC

ACF = Antonio Carlos Fernandes – LOC

FR = Felipe Ribeiro – SS7

Documented Information	DI – [Document Initials]
Template version	0
Authors	Daniel de Oliveira Costa Rafaela Sabrina Carneiro
Approved by	Antonio Carlos Fernandes
Issue [aaaa/mm/dd]	2021/12/10



Laboratório de
Ondas e Correntes
COPPE|UFRJ

This document corresponds to an internal report referring to a procedure performed at the Laboratory of Waves and Currents (LOC – COPPE/UFRJ) and all rights are reserved thereto. Any partial or full reproduction of the contents in this report without proper authorization is prohibited, under penalty of adopting appropriate measures in the civil and criminal spheres if necessary.

TABLE OF CONTENTS

1.	Introduction	7
2.	Summary of experimental setup.....	8
2.1.	Normal oscillations at 1:30 scale.....	8
2.2.	Axial oscillations at 1:30 scale	9
2.3.	Normal and axial oscillations at 1:9 scale	11
2.4.	Effect of model's rotation	11
3.	Overview of experimental data	13
3.1.	Typical time series	13
3.2.	Repeatability analysis.....	16
3.3.	Effect of model's axial rotation.....	18
4.	Procedure for data analysis	21
4.1.	Overview	21
4.2.	Filtering	22
4.3.	Synching.....	23
4.4.	Data adjustment to calculate hydrodynamic coefficients	24
5.	GJR hydrodynamic coefficients	25
5.1.	1:9 scale.....	25
5.1.1.	Normal oscillations at 1:9 scale.....	25
5.1.2.	Axial oscillations at 1:9 scale	28
5.1.3.	Effect of model rotation	31
5.1.4.	Effect of model porosity.....	32
5.2.	1:30 scale.....	33
5.2.1.	Normal oscillation at 1:30 scale	33
5.2.2.	Axial oscillation at 1:30 scale	35
5.2.3.	Effect of model porosity.....	37
5.3.	Final comments on the results	38
6.	References	39
	Appendix A. Repeatability analysis.....	40
A.1.	Axial oscillations at 1:9 scale.....	40
A.2.	Normal oscillations at 1:9 scale	43
A.3.	Axial oscillations at 1:30 scale – 1 st set of tests	45
A.4.	Normal oscillations at 1:30 scale – 1 st set of tests	48
A.5.	Axial oscillations at 1:30 scale – 2 nd set of tests	51

A.6. Normal oscillations at 1:30 scale – 2 nd set of tests	54
---	----

1. Introduction

This document presents a report on the experimental analysis corresponding to the set of model tests carried out at the Visualization Tank in LOC for the hydrodynamic tests of forced oscillations of rigid models of the Gimbal Joint Riser (GJR) at two different scales, 1:9 and 1:30. The full test matrix and test conditions are presented, as designed, at the Test Request Forms ([1] and [2]) and in the Test Procedures Report [3]. The assemblies for both scales are summarized at the Experimental Setup Report [4]. The Model Test Report [5] presents the details corresponding to the model tests, data log, and repeatability analysis. These reports were previously emitted to client.

This report briefly summarizes the assemblies provided, as well as the test matrix, followed by the typical timeseries acquired by each sensor. The procedure for post-processing of the data is discussed, and main results of the experimental analysis are summarized in Chapter 5.

2. Summary of experimental setup

This section briefly reviews the experimental setup provided for the tests in both scales. More details in [4]. The tests consisted of forced oscillations of the GJR model in two different directions, one aligned to its length (axial oscillation) and the other perpendicular to its length (normal case).

2.1.Normal oscillations at 1:30 scale

Figure 2-1 displays schematic drawing of the assembly with measurements taken from the setup illustrated by Figure 2-2, which displays pictures of the actual setup highlighting important sensors and components. Table 2-1 lists all components used in this assembly with their masses.

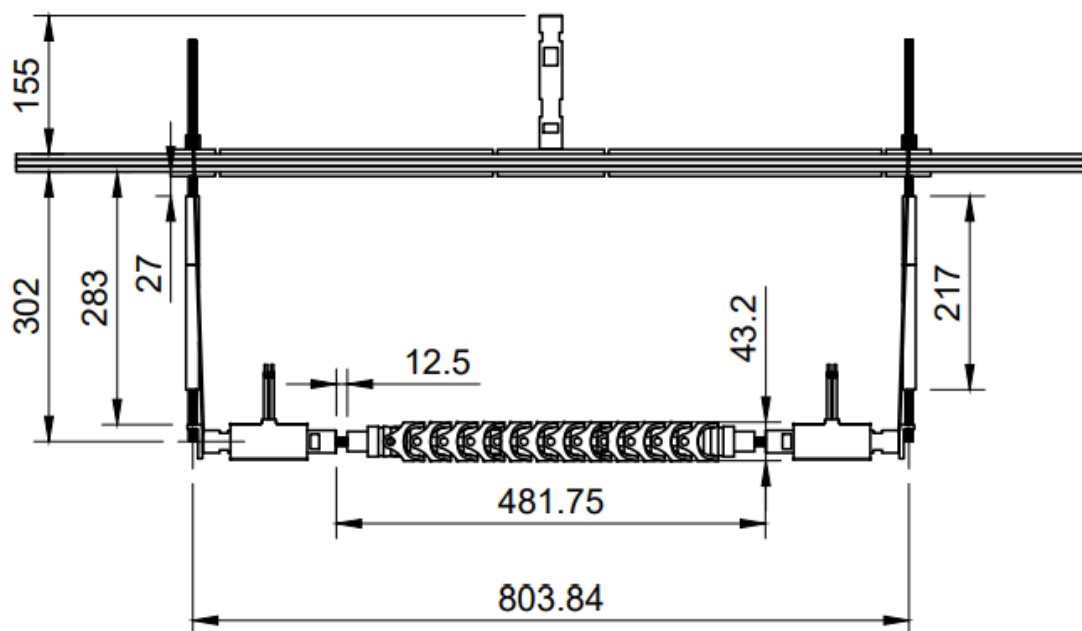


Figure 2-1: Schematic drawing of the 1:30 setup for the normal oscillation conditions zooming at the supporting structure (dimensions in mm)

Table 2-1: List of components in normal oscillation assemblies at 1:30 scale

Component	Mass (kg)
20x20 mm structural beams	1.437
NACA0018+rod (each)	0.299
Cable-staying system (each)	0.576
Top loadcell	0.899
Submerged loadcell (each)	0.899
Model	0.2995
TOTAL	6.184

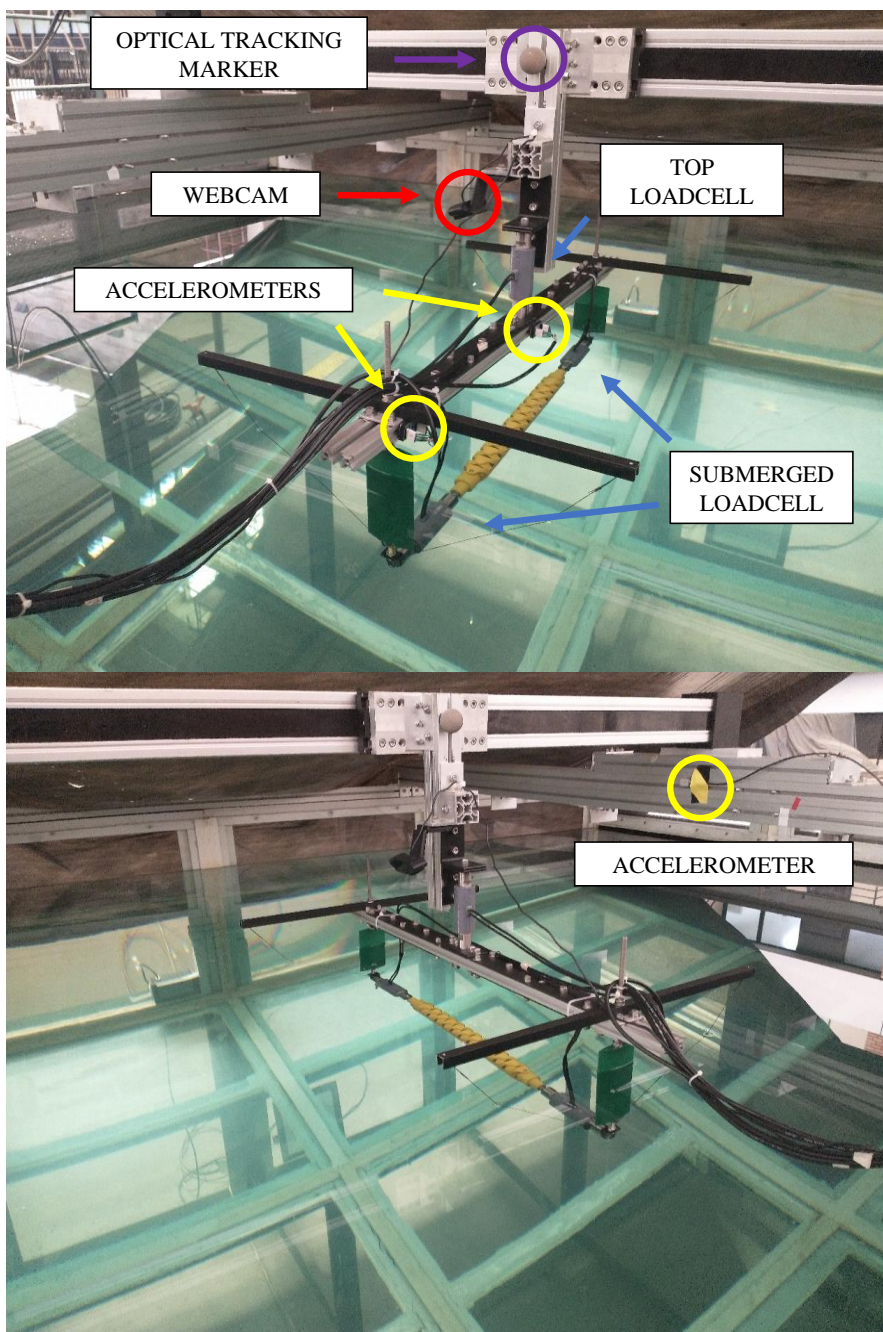


Figure 2-2: Experimental assembly for normal oscillations at 1:30 scale – close view

2.2.Axial oscillations at 1:30 scale

Figure 2-3 displays schematic drawing of the assembly with measurements taken from the setup illustrated by Figure 2-4, which displays pictures of the actual setup highlighting important sensors and components. Table 2-2 lists all components used in this assembly with their masses.

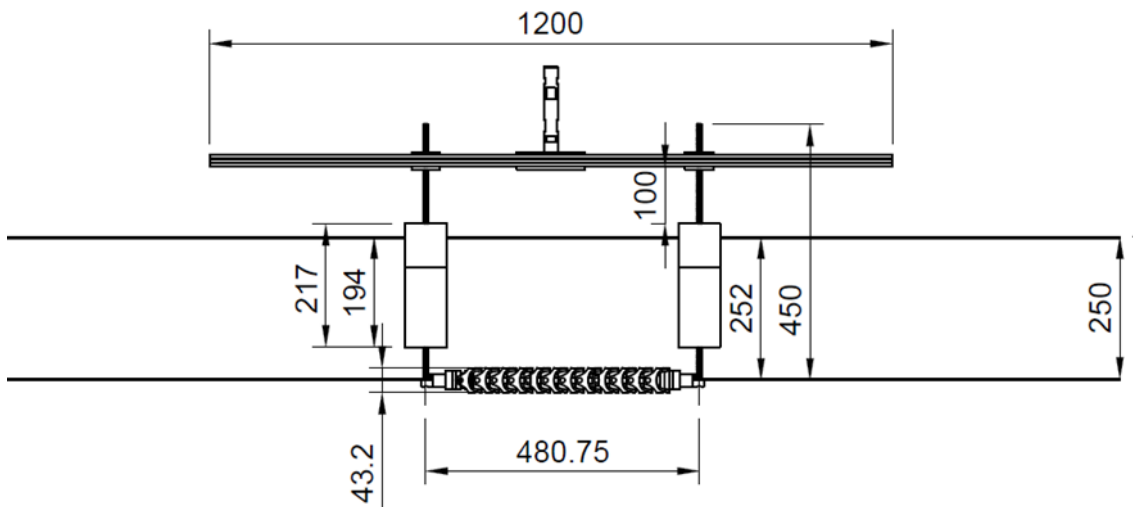


Figure 2-3: Schematic drawing of the 1:30 setup for the axial oscillation conditions zooming at the supporting structure (dimensions in mm)

Table 2-2: List of components in axial oscillation assemblies at 1:30 scale

Component	Mass (kg)
20x20 mm structural beams	1.437
NACA0018+rod (each)	0.299
Cable-staying system (each)	0.576
Top loadcell	0.899
Model	0.2995
TOTAL	4.386

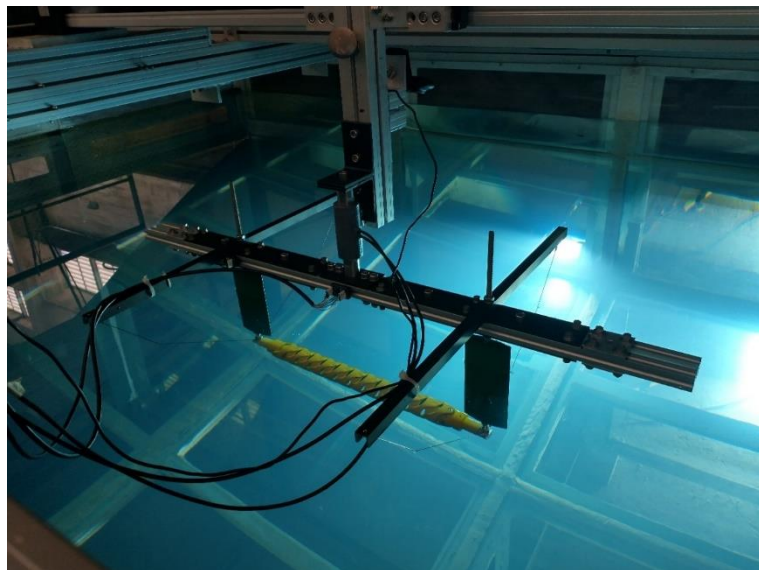


Figure 2-4: Experimental assembly for axial oscillations at 1:30 scale – close view

2.3.Normal and axial oscillations at 1:9 scale

The assembly at 1:9 scale slightly differs to that in 1:30 scale, switching from a single point support to a dual support structure, as illustrated by Figure 2-5. The same components were used in both axial and normal conditions, opposed to the 1:30 scale in which the submerged loadcells were removed for the axial oscillations.



Figure 2-5: Schematic drawing of the 1:9 setup for the normal oscillation conditions

Table 2-3: List of components in axial and normal oscillation assemblies at 1:9 scale

Component	Mass (kg)
Set of 3 50x50 mm structural beams (1)	11.340
Dual support with top loadcell (2)	4.710
Cable-staying system – each (3)	0.830
NACA0018+tube – each (4)	2.450
Submerged loadcell – each (5)	0.899
Model	5.110
TOTAL	29.518

2.4.Effect of model's rotation

In the premises of the test [6] of the hydrodynamic tests, it was defined the GJR model was to be tested in two different conditions, one of the model at 00DEG and the second with the model rotated by 45 degrees around its axis to verify any effect of the angle of the body segments over the hydrodynamic loads. Figure 2-6 illustrates the difference, which was tested in both scales and both oscillation conditions (axial and normal).



Figure 2-6: Different angles in which the GJR model was tested

3. Overview of experimental data

This chapter briefly overviews the experimental data as acquired during the tests at both 1:9 and 1:30 scales. Typical time series are displayed, and the stationary state is characterized. A summary of repeatability analysis is presented in this chapter and in details in Appendix A.

3.1.Typical time series

Figure 3-1 illustrates the typical time series acquired during the first set axial excitation at 1:30 scale, showing the imposed motion at the upper plot and the load as measured by the top loadcell at the lower plot. The image compares the raw to the filtered data in both graphs, using a 4th order Butterworth low-pass filter with a cutoff frequency of 5 Hz, 6 times larger than the greater frequency to be tested (0.83 Hz or 1.2 s in period). The upper plot shows the filtered data overlaps the raw time series, while the lower graph shows the noisy behavior in the load shortly after the beginning of the motion. This noisy behavior relates to the structural vibration due to the bump, and normally vanishes after a few cycles as illustrated by the lower plot, showing the overlap of the filtered and raw time series for the load after 10 s.

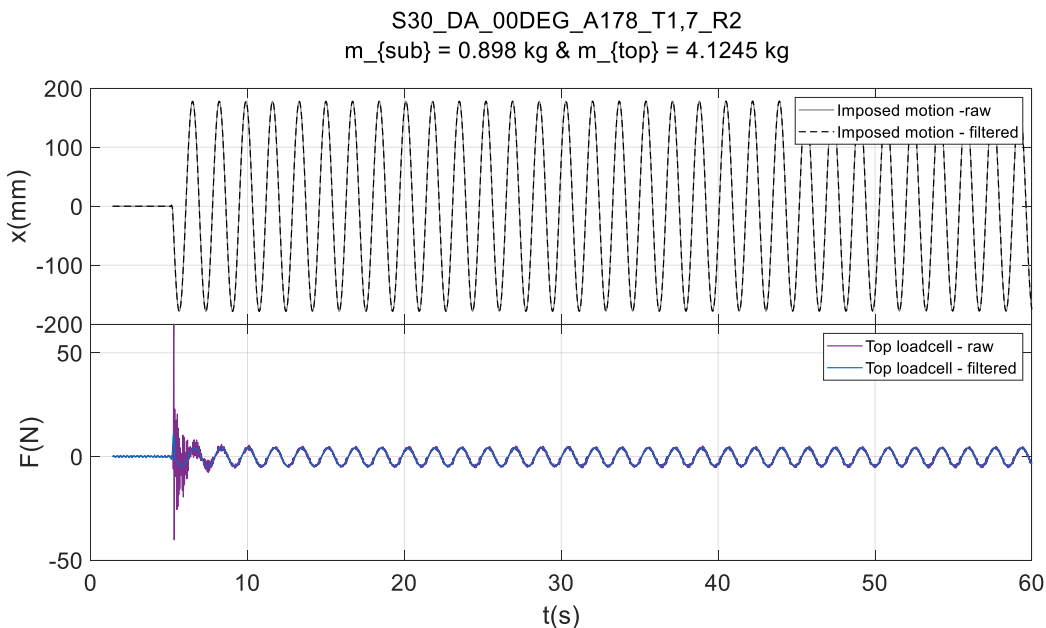


Figure 3-1: Time series for motion (upper) and load (lower)

To better visualize this relation, Figure 3-2 presents the spectral density plot corresponding to the time series of load, displayed above, calculated through a simple FFT (Fast Fourier Transform) for the first cycles after the beginning of the imposed motion until 10 s. The FFT shows the first peak frequency matches the oscillation imposed, and additional peaks are observed for larger frequencies, specially within the bandwidth of frequencies noticed for the PMM and the structural response during hammer tests [4].

Figure 3-3 extends the analysis showing the FFT of load calculated for different intervals, starting with the first cycle of oscillation, which shows significant energy in large frequencies, after the first cycle and before 10 s, showing significantly less energy, and after 10 s, with nearly no energy in frequencies other than the imposed. This effect is naturally more intense for

larger accelerations (larger frequencies and amplitudes) but was observed in all cases. This analysis reinforces the 5 Hz adopted for the cutoff frequency for the low-pass filter.

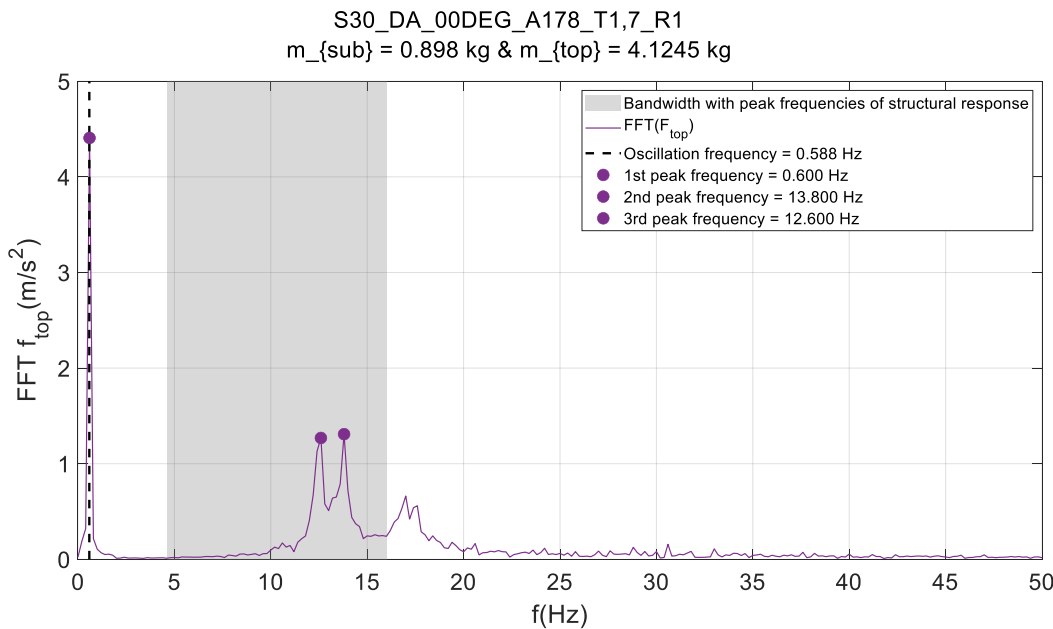


Figure 3-2: Power spectrum density of load right after beginning of motion

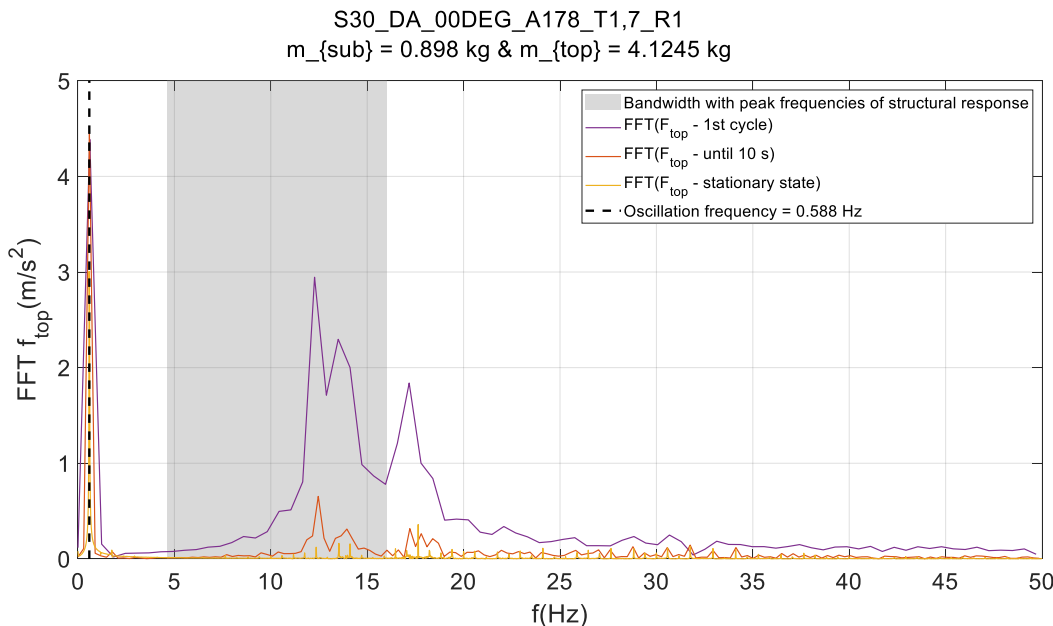


Figure 3-3: Power spectrum density of load right at different moments

Figure 3-4 displays the time series corresponding to the case with 178 mm in amplitude and 1.7 s in period. In this figure, the upper plot shows the time series of motion of the run with the model, while the 2nd plot displays the motion of the run with the structure alone, without the model. The harmonic behavior in the imposed motion is clear given the sinusoidal shape in both plots. The comparison of both shows at first a desynchronization, which is a consequence of manually starting the motion during each run. Nevertheless, the amplitudes in both runs are

nearly the same, as shown by the legends in each plot (177.93 mm and 178.17 mm, respectively). This points to the need of a synchronization procedure at the post-processing of the data, so that the comparison between the data with and without the model is properly performed.

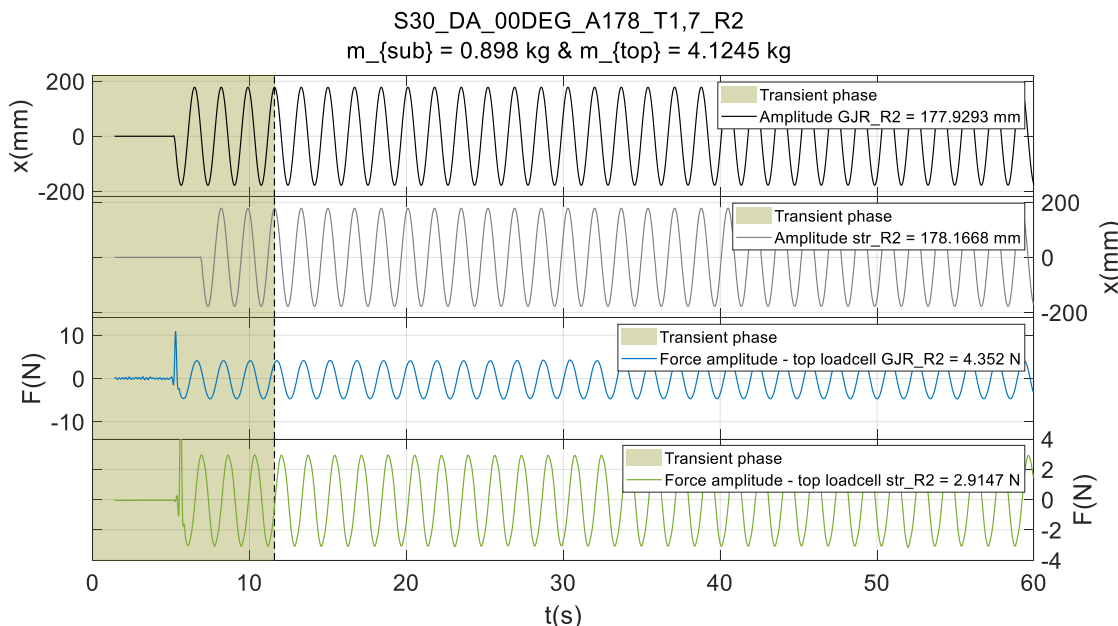


Figure 3-4: Time series of motion of the model (1st plot), motion of the structure alone (2nd plot) and the loads corresponding to both in axial oscillation at 1:30 scale

The image above also presents the time series of load as acquired by the top loadcell in both cases, with and without the model at the 3rd and 4th plots, respectively. The first aspect that stands out in both plots is the abrupt increase in load due to the bump at the beginning of the motion. This bump, in turn, is evident when observing how the time series of motion starts right away as a harmonic function, without a smooth acceleration.

Generally, the typical behavior in normal oscillation is very similar to what was presented for the axial excitation. The major difference to the previous case is the magnitude of the load, which is significantly more intense than the axial excitation.

The major difference noticed for the tests at 1:9 when compared to the 1:30 hereby illustrated is the magnitude of the loads and the time scale. Overall, the typical behavior pointed in this chapter holds for the larger model.

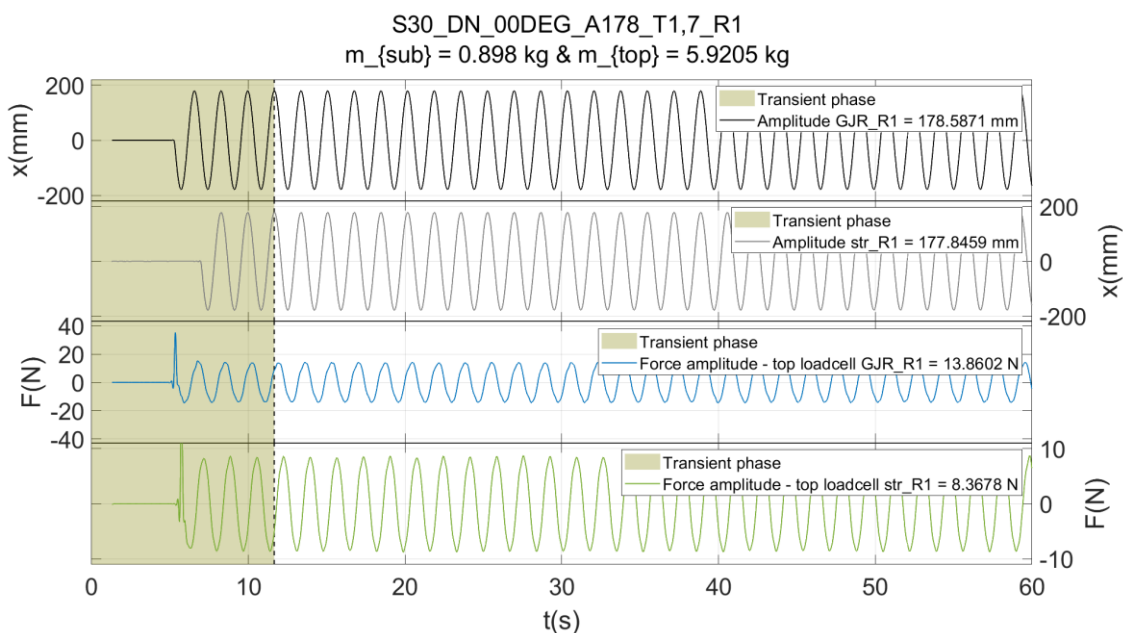


Figure 3-5: Time series of motion of the model (1st plot), motion of the structure alone (2nd plot) and the loads corresponding to both in normal oscillation at 1:30 scale

3.2.Repeatability analysis

As planned in the test matrix, each case was repeated thrice to check for repeatability. At this point, the most important parameter regarding this analysis is the comparison between equivalent runs. This was verified by calculating the amplitude of motion and of the load through the harmonic equivalent which, as shown in Equation (3.1), is proportional to the standard deviation of the time series and can be implemented to any signal (load or motion). Even knowing, as abovementioned, that in many cases the time series for the motion was not harmonic – although it was cyclic – this parameter provides a good indication of the ergodicity of the tests.

$$\text{amplitude} = \sqrt{2} \text{ std(signal)} \quad (3.1)$$

Figure 3-6 displays plots of both amplitude of motion and load as calculated through (3.1), the latter using the filtered signal. The amplitudes of motion are plotted as bars, while the load amplitude in a curve, for a better visualization of both parameters simultaneously. Each 3 consecutive points in the plot below represent the 3 runs of each case. One notices that the amplitude of motions does not vary significantly in each run. The amplitudes of load present slightly larger variation when compared to the motion, but still small enough to indicate repeatability of the test.

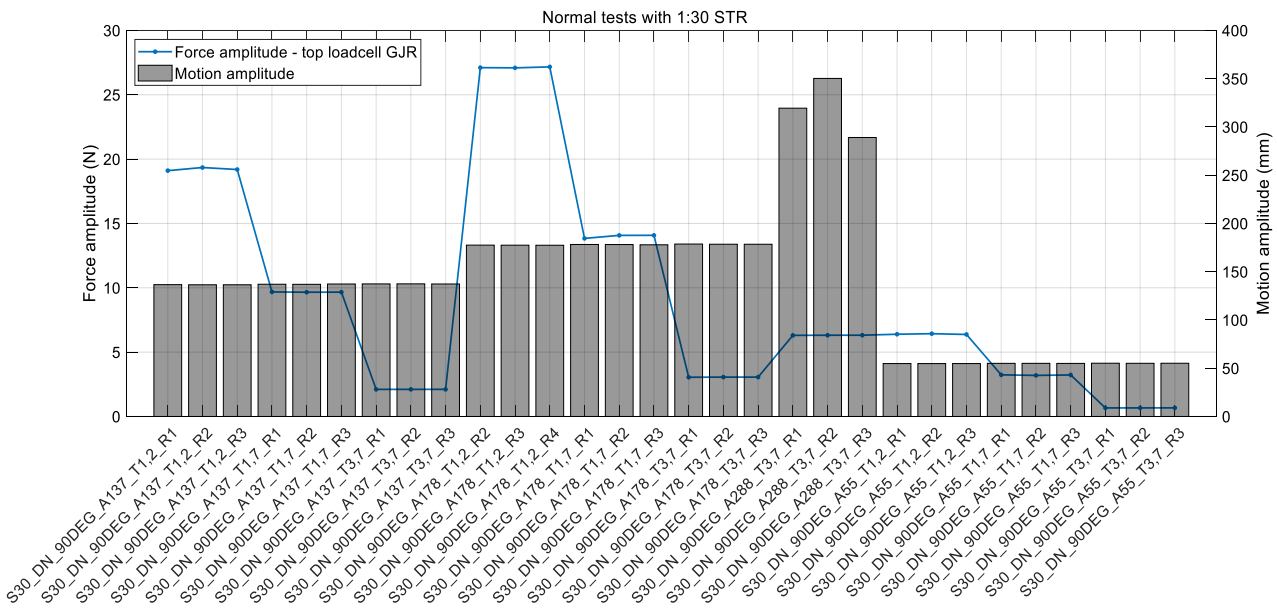


Figure 3-6: Amplitudes of motion (bars) and load (blue curve) in each run – repeatability check for normal oscillations at 90DEG at 1:30 scale

Table 3-1 presents the amplitudes of motion and load for each case, and the RMS error over the mean for each set of 3 runs. The error RMS over the mean value indicates a variation of less than 1% in all cases for the amplitude motion, while the variation in the load gets up to 5% with respect the mean value in some cases. The larger percentage, compared to what is observed for the motion, is due to the small mean value for the load, as seen below.

Table 3-1: Repeatability check for 1:30 normal oscillations at 90DEG

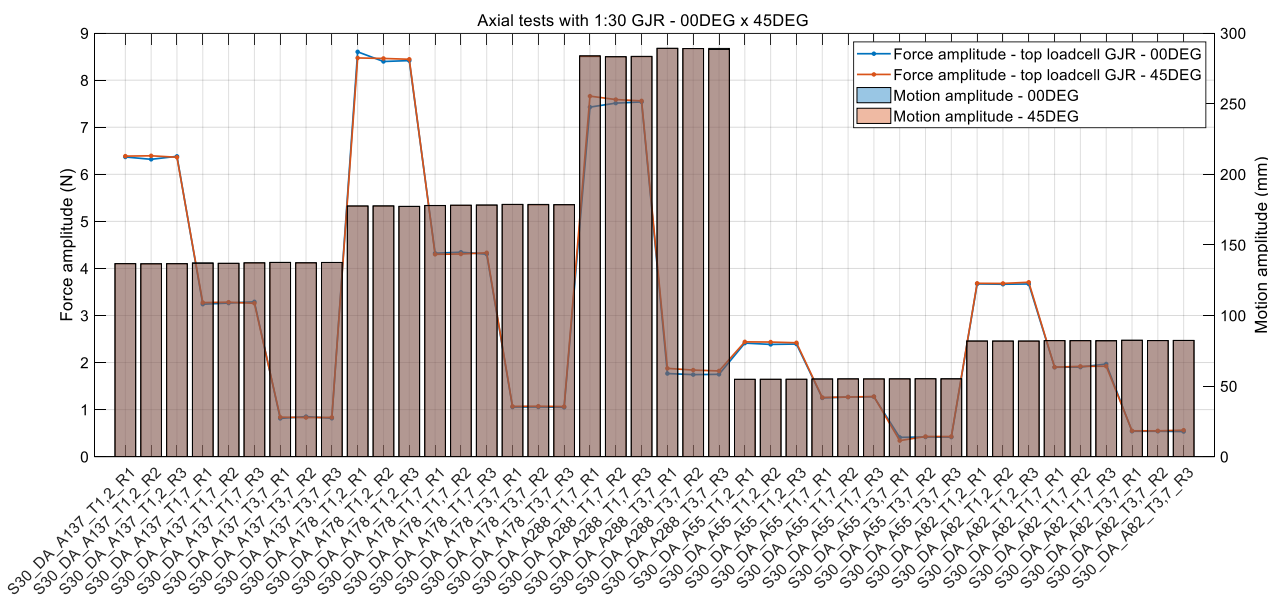
CASE	AMPLITUDE OF MOTION					AMPLITUDE OF LOAD				
	R1 (mm)	R2 (mm)	R3 (mm)	MEAN (mm)	ERROR RMS %	R1 (N)	R2 (N)	R3 (N)	MEAN (N)	ERROR RMS %
S30_DN_90DEG_A55_T1,2	54.83	54.82	54.83	54.83	0.01%	6.39	6.43	6.37	6.40	0.40%
S30_DN_90DEG_A82_T1,2	-	-	-	-	-	-	-	-	-	-
S30_DN_90DEG_A137_T1,2	136.59	136.44	136.46	136.50	0.05%	19.10	19.35	19.19	19.21	0.52%
S30_DN_90DEG_A178_T1,2	177.54	177.48	177.41	177.47	0.03%	27.11	27.09	27.17	27.12	0.12%
S30_DN_90DEG_A288_T1,2	-	-	-	-	-	-	-	-	-	-
S30_DN_90DEG_A55_T1,7	55.04	55.06	54.99	55.03	0.05%	3.24	3.19	3.23	3.22	0.58%
S30_DN_90DEG_A82_T1,7	82.20	82.04	82.01	82.08	0.10%	5.03	5.04	5.03	5.04	0.09%
S30_DN_90DEG_A137_T1,7	137.01	136.93	137.27	137.07	0.10%	9.68	9.66	9.66	9.67	0.10%
S30_DN_90DEG_A178_T1,7	178.20	178.15	177.88	178.08	0.08%	13.84	14.07	14.08	14.00	0.80%
S30_DN_90DEG_A288_T1,7	-	-	-	-	-	-	-	-	-	-
S30_DN_90DEG_A55_T3,7	55.18	55.09	55.15	55.14	0.07%	0.67	0.67	0.67	0.67	0.21%
S30_DN_90DEG_A82_T3,7	82.33	82.23	82.18	82.25	0.07%	1.07	1.07	1.07	1.07	0.03%
S30_DN_90DEG_A137_T3,7	137.35	137.41	137.28	137.35	0.04%	2.11	2.11	2.11	2.11	0.05%
S30_DN_90DEG_A178_T3,7	178.65	178.46	178.44	178.52	0.05%	3.05	3.06	3.06	3.06	0.17%
S30_DN_90DEG_A288_T3,7	319.43	350.24	289.06	319.58	7.82%	6.30	6.31	6.32	6.31	0.09%

This analysis was performed for both scales and all conditions, with the GJR model and without it. Appendix A presents the plots and tables corresponding to each case in details.

3.3. Effect of model's axial rotation

Overall, when comparing the mean values for the amplitudes of motion and load for the model in different angles one notices small variations for both, indicating the orientation in which the model is excited does not affect the hydrodynamic loads. Figure 2-6 displays the difference between both conditions.

Figure 3-7 compares the amplitudes of motion and load through the same type of graph presented above but overlapping the cases at 0 deg at after rotated by 45 degrees for the normal oscillation, clearly showing the resemblance in both curves, and indicating that the angle in which the gimbal is oscillated does not affect the hydrodynamic load acting on it. Figure 3-8 shows that rotating the model does not affect the magnitude of load on the model neither. Finally, an additional case of the model rotated by 90 degrees was tested, as in Figure 3-9, leading to the same conclusion that the rotation of the model does not seem to affect the hydrodynamic load on the GJR model. Similar behavior was observed at the 1:9 cases, as illustrated by Figure 3-10.



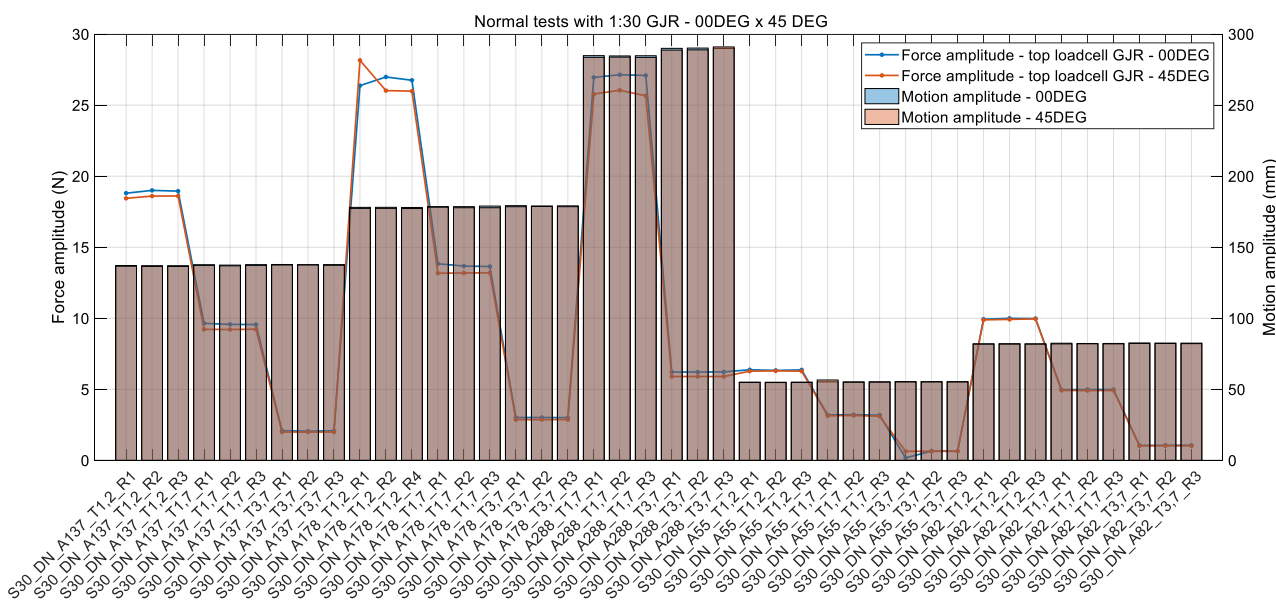


Figure 3-8: Repeatability check for normal oscillations at 00DEG x 45DEG at 1:30 scale

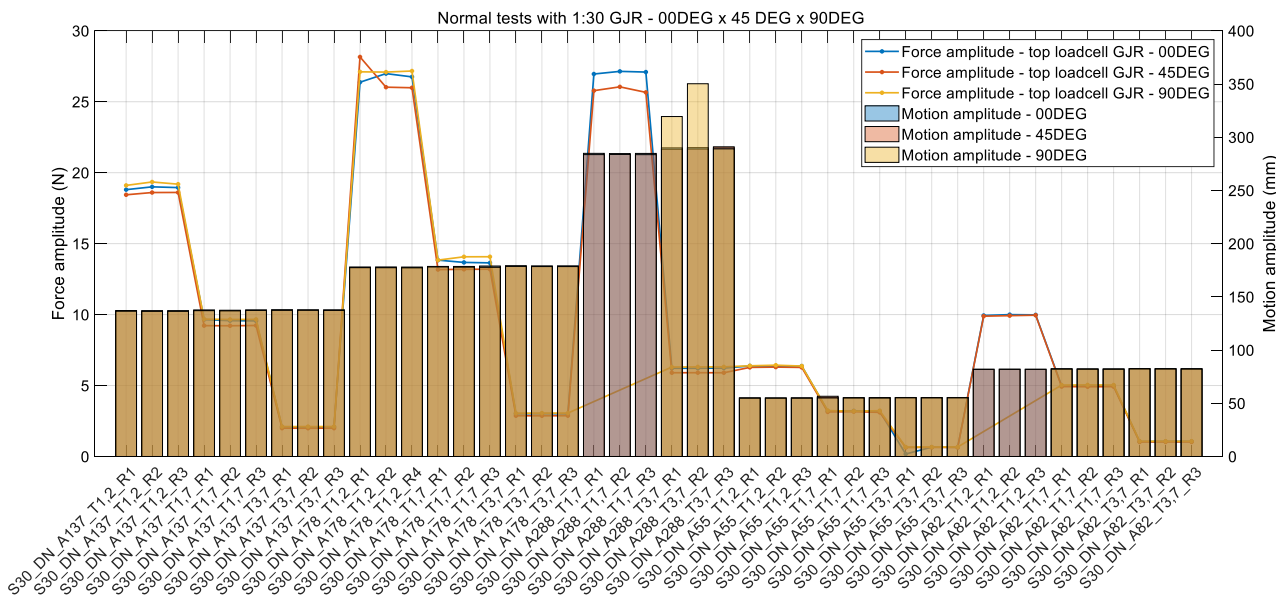


Figure 3-9: Repeatability check for normal oscillations at 00DEG x 45DEG x 90DEG at 1:30 scale

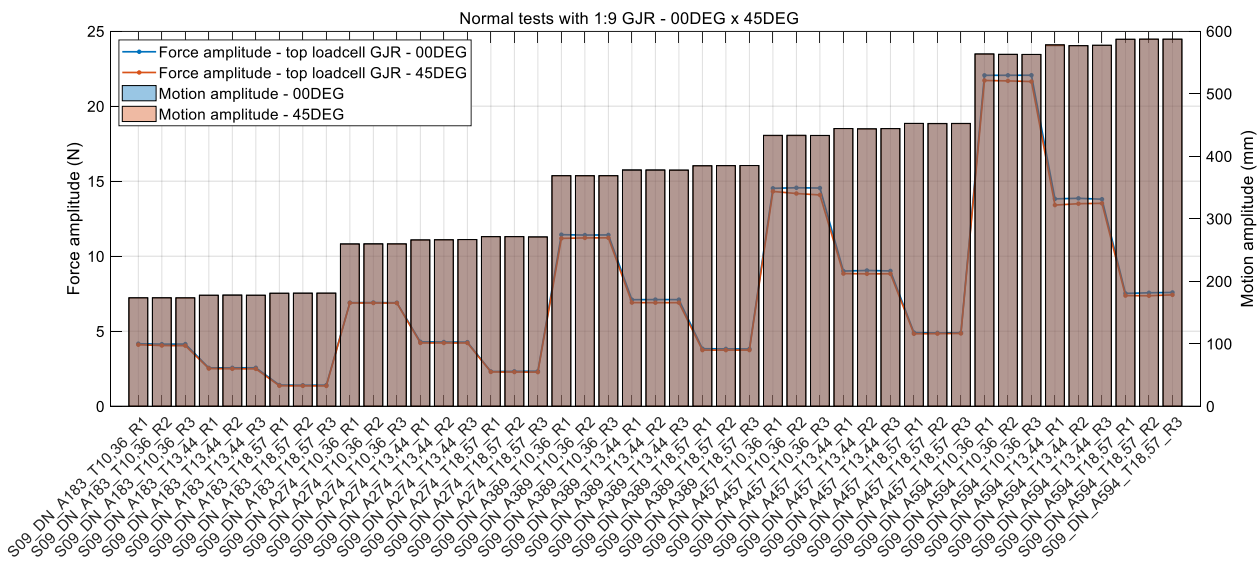


Figure 3-10: Repeatability check for normal oscillations at 00DEG x 45DEG at 1:9 scale

4. Procedure for data analysis

This chapter covers the procedures for the post processing of the experimental data to calculate the hydrodynamic coefficients for the GJR. The procedures hereby discussed were adopted for both scales. The sessions below describe each session individually, after introducing an overview of the entire procedure.

4.1. Overview

The goal of the tests is to estimate the hydrodynamic coefficients of the GJR based on forced oscillations of rigid scaled models. As illustrated in chapter 2, the experimental assembly designed for this test consists of a support holding the model, which in turn is attached to the oscillator. Consequently, as illustrated in Figure 4-1, during the forced oscillation different load components act on the model-support set. On the GJR, the loads can be split off into hydrodynamic (F_H^{GJR}) and inertial (F_I^{GJR}). Analogously, the loads acting on the supporting structure can be divided both in terms of hydrodynamic (F_H^{STR}) and inertial (F_I^{STR}) as well. For the top loadcell, since the measurement is taken in a non-inertial reference frame, the inertial correction on the sensor (F_I^{LC}) must be considered as well.

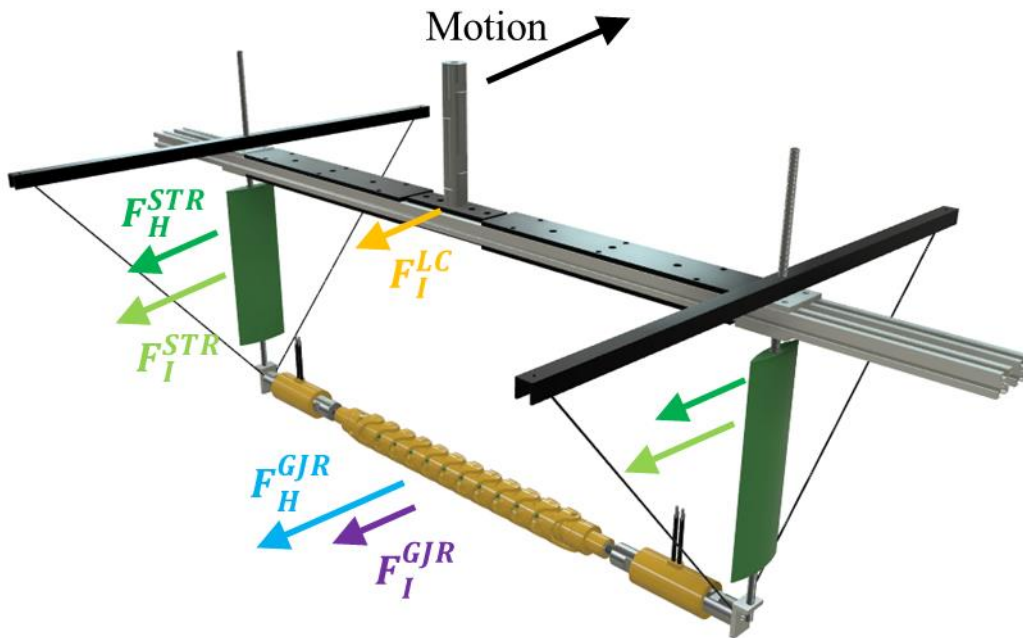


Figure 4-1: Free body diagram of the model during forced oscillation

Consequently, the total load acquired during the test by the top loadcell can be assumed to be the sum of all components above mentioned, as in (4.1).

$$F_{TOTAL}^{TOP} = F_H^{GJR} + F_I^{GJR} + F_H^{STR} + F_I^{STR} + F_I^{LC} \quad (4.1)$$

As mentioned in chapter 2, for each different condition the tests were performed with and without the GJR model. Hence, as in the free body diagrams in Figure 4-2, it is possible to subtract the inertial and hydrodynamic loads on the structure, as well as the inertial effects on

the loadcell, by relating the time series from both measurements. It is then possible to calculate the hydrodynamic loads acting on the GJR as in (4.2).

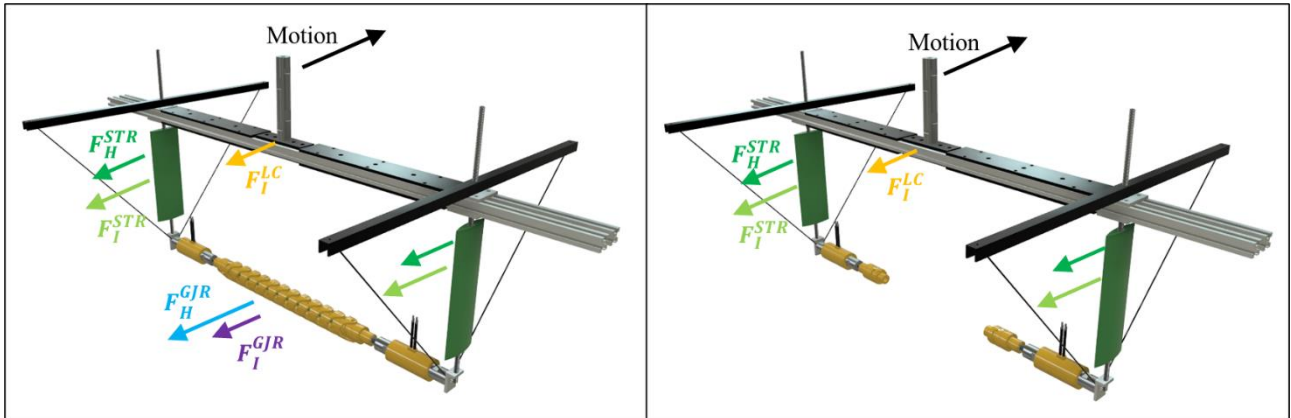


Figure 4-2: Free body diagram of tests with (left) and without (right) GJR

$$F_H^{GJR} = F_{TOTAL}^{TOP} - F_{TOTAL}^{TOP**} - F_I^{GJR} = F_{TOTAL}^{TOP} - F_{TOTAL}^{TOP**} - m_{GJR} \ddot{x} \quad (4.2)$$

Where:

- F_H^{GJR} Hydrodynamic load acting on the GJR model as measured, to be decomposed on drag and inertia components (see (4.3))
- F_{TOTAL}^{TOP} Time series of load as acquired during the tests with GJR model
- F_{TOTAL}^{TOP**} Time series of load as acquired during the tests without GJR model
- F_I^{GJR} Inertial loads acting on the GJR model
- m_{GJR} GJR mass
- \ddot{x} GJR acceleration

4.2. Filtering

As discussed in chapter 3, the tests were carried out at a 100 Hz sampling rate. Noise can then be noticed in the time series, for instance in Figure 3-1. In the post processing of the data a low-pass digital filter was implemented to remove such effects, more specifically, a 4th order Butterworth filter, which is usually selected due to efficiently attenuating effects in the stopband without ripples either in the passband or stopband. However, when compared to other types of filters such as the elliptic, this type of filter does present a somewhat wide transition band, that is the bandwidth of frequencies after the cutoff frequency which are not fully attenuated. This means that the cutoff frequency must be properly selected to fully filter high frequency features in the time series without any reminiscent effect passing through it.

A cutoff frequency 5 times larger than the excitation frequency was selected. Figure 3-2 and Figure 3-3 illustrated the validity of the cutoff frequency selected, already in the range of structural response of the model-support set and significantly above the excitation frequency. Figure 4-3 displays the comparison between raw and filter data for the load acquired by the top loadcell for a 1:30 case as example of the effectiveness of the type of filter adopted.

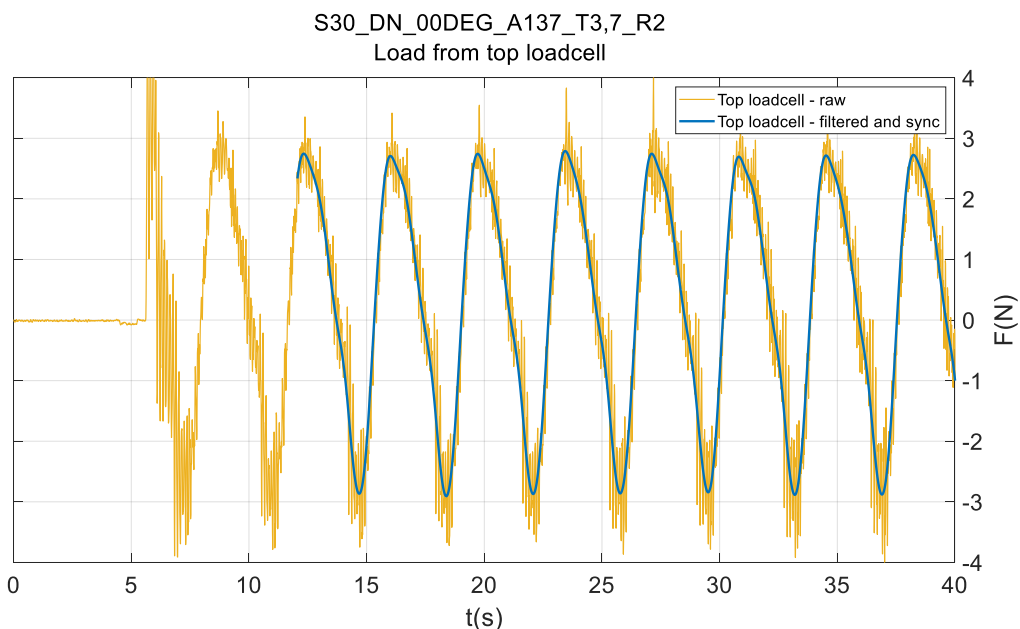


Figure 4-3: 4th order low-pass Butterworth filter effectiveness

4.3.Synching

Given equation (4.2), it is clear the importance of synchronizing time series from different and independent measurements. This can be done at the post-processing phase, by selecting easily identifiable events as synching triggers. The imposed motion, given its clear harmonic behavior, is the best candidate for such, by using the first peak of the signal after reaching stationary state as trigger event. For the sake of visualization, all 3 runs were set to the same time base using the same technique. Figure 4-4 displays the synching process for all runs of the same case, showing the imposed motion for the test with the GJR model at the upper plot and the motion of the structure alone, without the model, at the lower plot. The dashed lines represent the original unsynced signals and the full plots the synced time series, which are all overlapped.

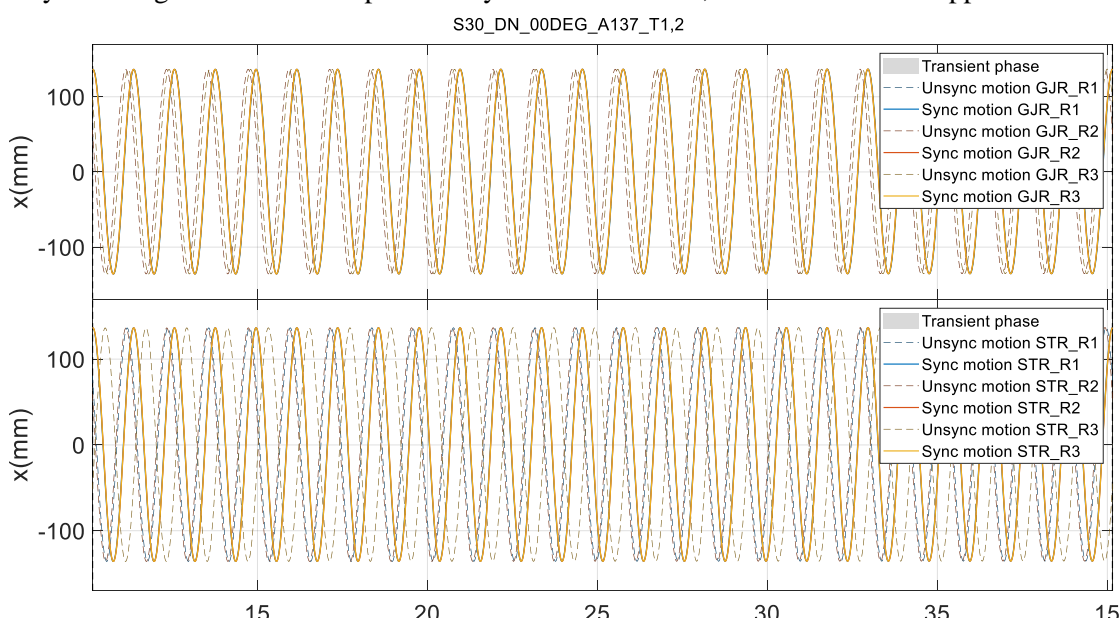


Figure 4-4: Example of synchronization of different time series

4.4.Data adjustment to calculate hydrodynamic coefficients

Once the hydrodynamic load is defined as in equation (4.2), properly synched and filtered, the hydrodynamic coefficients can be estimated through a simple adjustment to a generic expression following Morison's equation, as in (4.3) for an oscillated body in still water.

$$\mathbf{F}_H^{GJR}(t) = -C_A(KC, Re) \rho \nabla \ddot{x}(t) - C_D(KC, Re) \frac{1}{2} \rho S \dot{x}(t) |\dot{x}(t)| \quad (4.3)$$

Where:

$F_H^{GJR}(t)$	Hydrodynamic load acting on the GJR model as measured, to be decomposed on drag and inertia components (see (4.2))
C_A	Added mass coefficient, $C_A = C_M - 1$. It depends on KC and Re numbers.
C_D	Nondimensional drag coefficient. It depends on KC and Re numbers
ρ	Water density
∇	Submerged volume of GJR model
S	Reference area. Projected area for normal oscillations and surface area for axial oscillations
\ddot{x}	Imposed acceleration
\dot{x}	Imposed velocity
KC	Keulegan-Carpenter number, $KC = 2\pi A/D_{GJR}$
Re	Reynolds number, $Re = A\omega D_{GJR}/\nu$
A	Amplitude of motion
D_{GJR}	Diameter of GJR model
ω	Frequency of oscillation, $\omega = 2\pi/T$

The velocity ($\dot{x}(t)$) and acceleration ($\ddot{x}(t)$) can be differentiated from the imposed motion ($x(t)$). According to ITTC recommendations [7], the water density is taken as 998.20 kg/m^3 , which is around the same value as usually measured in the lab.

The first load component in (4.3) represents the hydrodynamic reactions to the acceleration imposed, hence named the inertial load. The coefficient C_A is the nondimensional added mass, related to the inertia coefficient (C_M). The second load component is the drag force is proportional to a characteristic area. For the normal oscillations it is taken as the projected area ($S = L_{GJR} D_{GJR}$), while for the axial oscillation it is taken as the surface area of the surrounding cylinder ($S = \pi D_{GJR} L_{GJR}$).

A simple least-squares adjustment can be used to estimate the hydrodynamic coefficients from the time series of load, velocity, and acceleration, as in [8].

5. GJR hydrodynamic coefficients

This chapter covers the results of the experiments of the GJR in both scales in terms of the hydrodynamic coefficients. For cases with normal oscillation the values are compared to classic data from literature [8].

5.1.1:9 scale

5.1.1. Normal oscillations at 1:9 scale

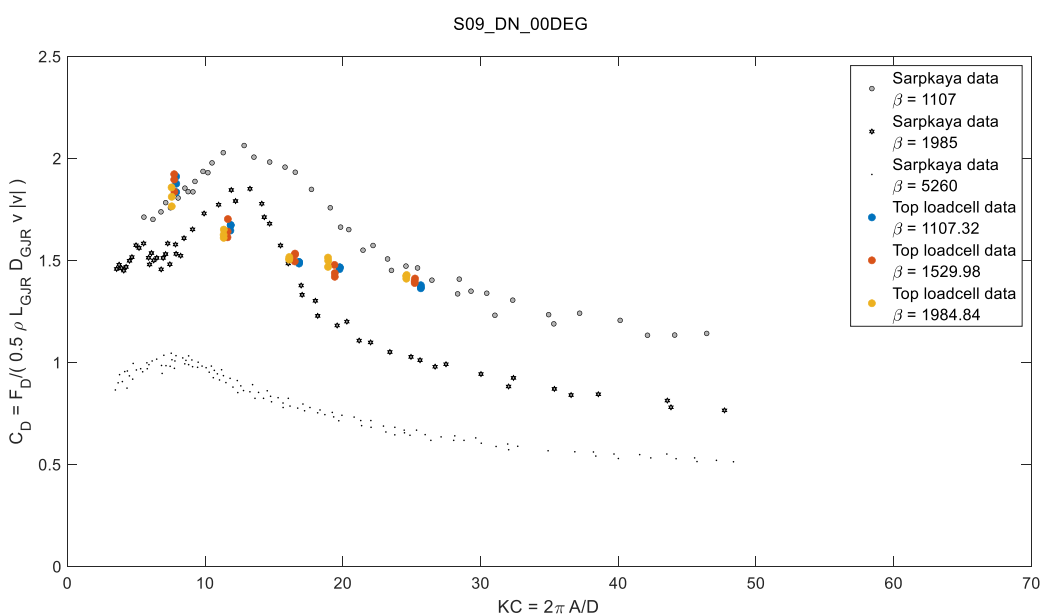


Figure 5-1: Drag coefficient x KC number for the normal oscillation at 1:9 scale at 00DEG

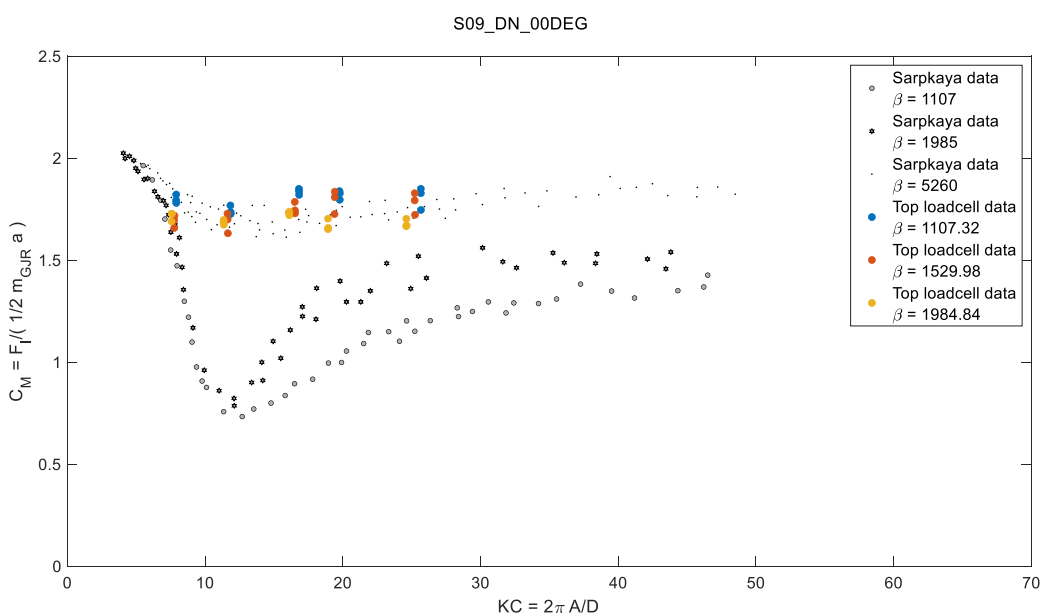


Figure 5-2: Inertia coefficient x KC number for the normal oscillation at 1:9 scale at 00DEG

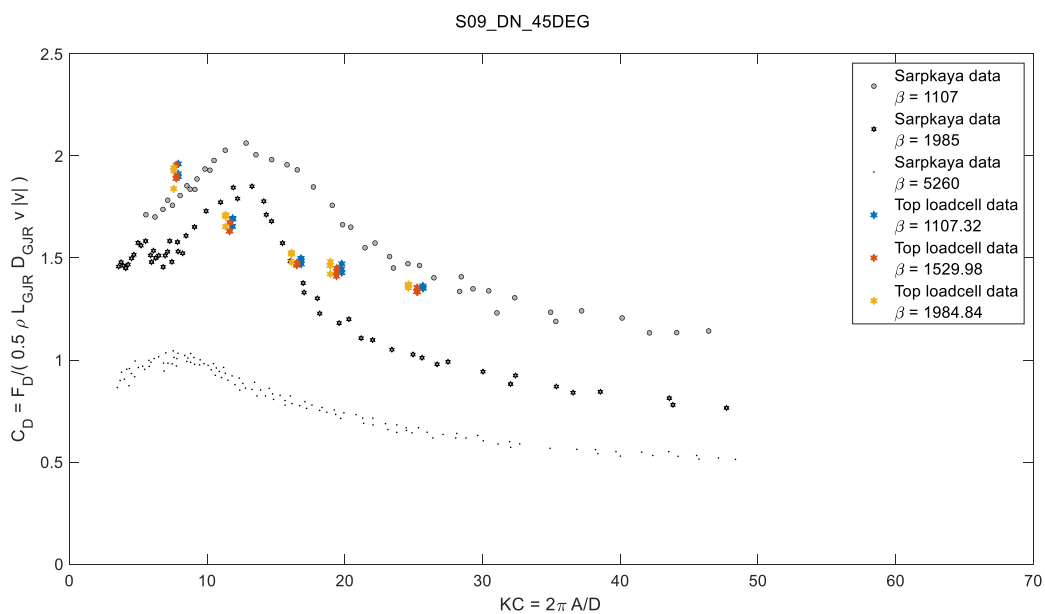


Figure 5-3: Drag coefficient x KC number for the normal oscillation at 1:9 scale at 45DEG

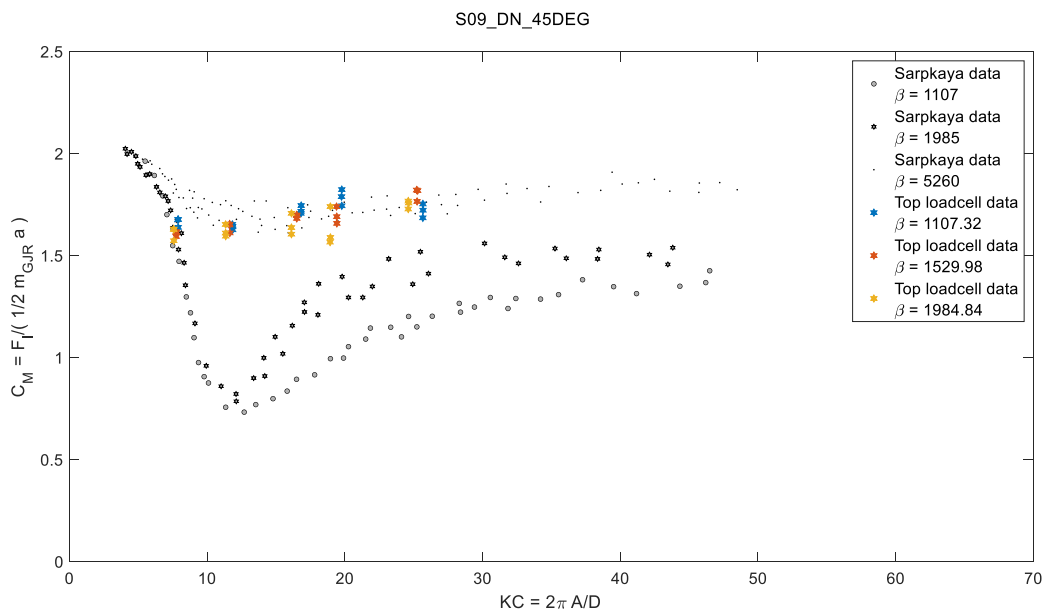


Figure 5-4: Inertia coefficient x KC number for the normal oscillation at 1:9 scale at 45DEG

These plots show the independence of both C_D and C_M to the oscillatory Reynolds number, represented by the β .

Table 5-1: Drag coefficient x KC number for the normal oscillation at 1:9 scale at 00DEG and 45DEG

CASE		CD at 00 DEG					CD at 45 DEG				
β	KC	R1 (-)	R2 (-)	R3 (-)	MEAN (-)	ERROR RMS %	R1 (-)	R2 (-)	R3 (-)	MEAN (-)	ERROR RMS %
1984.84	7.58	1.81	1.76	1.86	1.81	2.09%	1.93	1.84	1.94	1.90	2.41%
1529.98	7.76	1.92	1.84	1.90	1.88	1.91%	1.96	1.91	1.89	1.92	1.47%
1107.32	7.90	1.91	1.88	1.83	1.87	1.67%	1.91	1.90	1.96	1.92	1.40%
1984.84	11.35	1.61	1.65	1.63	1.63	1.02%	1.65	1.70	1.71	1.69	1.51%
1529.98	11.63	1.61	1.64	1.70	1.65	2.26%	1.63	1.63	1.67	1.65	1.18%
1107.32	11.86	1.67	1.67	1.65	1.66	0.76%	1.69	1.69	1.65	1.68	1.07%
1984.84	16.12	1.52	1.50	1.51	1.51	0.36%	1.53	1.52	1.48	1.51	1.34%
1529.98	16.53	1.53	1.53	1.49	1.52	1.12%	1.47	1.48	1.46	1.47	0.34%
1107.32	16.82	1.49	1.48	1.49	1.49	0.23%	1.50	1.49	1.47	1.49	0.77%
1984.84	18.93	1.47	1.51	1.50	1.49	1.27%	1.42	1.48	1.46	1.46	1.72%
1529.98	19.42	1.42	1.48	1.44	1.45	1.68%	1.45	1.41	1.43	1.43	1.12%
1107.32	19.78	1.47	1.47	1.46	1.46	0.27%	1.43	1.45	1.47	1.45	1.23%
1984.84	24.64	1.43	1.41	1.42	1.42	0.53%	1.37	1.35	1.37	1.36	0.48%
1529.98	25.23	1.39	1.40	1.41	1.40	0.65%	1.33	1.33	1.36	1.34	0.73%
1107.32	25.67	1.36	1.38	1.37	1.37	0.45%	1.36	1.35	1.35	1.36	0.37%

Table 5-2: Inertia coefficient x KC number for the normal oscillation at 1:9 scale at 00DEG and 45DEG

CASE		CM at 00 DEG					CM at 45 DEG				
β	KC	R1 (-)	R2 (-)	R3 (-)	MEAN (-)	ERROR RMS %	R1 (-)	R2 (-)	R3 (-)	MEAN (-)	ERROR RMS %
1984.84	7.58	1.73	1.73	1.69	1.71	1.03%	1.63	1.63	1.57	1.61	1.65%
1529.98	7.76	1.66	1.72	1.70	1.69	1.46%	1.59	1.61	1.62	1.61	0.64%
1107.32	7.90	1.79	1.78	1.82	1.80	0.96%	1.68	1.68	1.64	1.66	1.10%
1984.84	11.35	1.70	1.67	1.68	1.68	0.55%	1.65	1.61	1.60	1.62	1.50%
1529.98	11.63	1.73	1.70	1.63	1.69	2.39%	1.65	1.66	1.61	1.64	1.19%
1107.32	11.86	1.73	1.73	1.77	1.74	1.03%	1.64	1.63	1.65	1.64	0.66%
1984.84	16.12	1.72	1.74	1.73	1.73	0.41%	1.61	1.64	1.71	1.65	2.58%
1529.98	16.53	1.73	1.74	1.79	1.75	1.36%	1.70	1.68	1.70	1.69	0.43%
1107.32	16.82	1.85	1.84	1.82	1.84	0.66%	1.71	1.72	1.75	1.72	0.94%
1984.84	18.93	1.70	1.65	1.66	1.67	1.37%	1.74	1.59	1.57	1.63	4.74%
1529.98	19.42	1.84	1.73	1.81	1.79	2.61%	1.66	1.74	1.69	1.70	1.99%
1107.32	19.78	1.83	1.80	1.84	1.82	0.97%	1.82	1.79	1.74	1.79	1.82%
1984.84	24.64	1.67	1.70	1.67	1.68	0.98%	1.76	1.77	1.73	1.75	0.95%
1529.98	25.23	1.83	1.79	1.72	1.78	2.46%	1.82	1.82	1.77	1.80	1.43%
1107.32	25.67	1.85	1.83	1.75	1.81	2.48%	1.69	1.72	1.75	1.72	1.62%

5.1.2. Axial oscillations at 1:9 scale

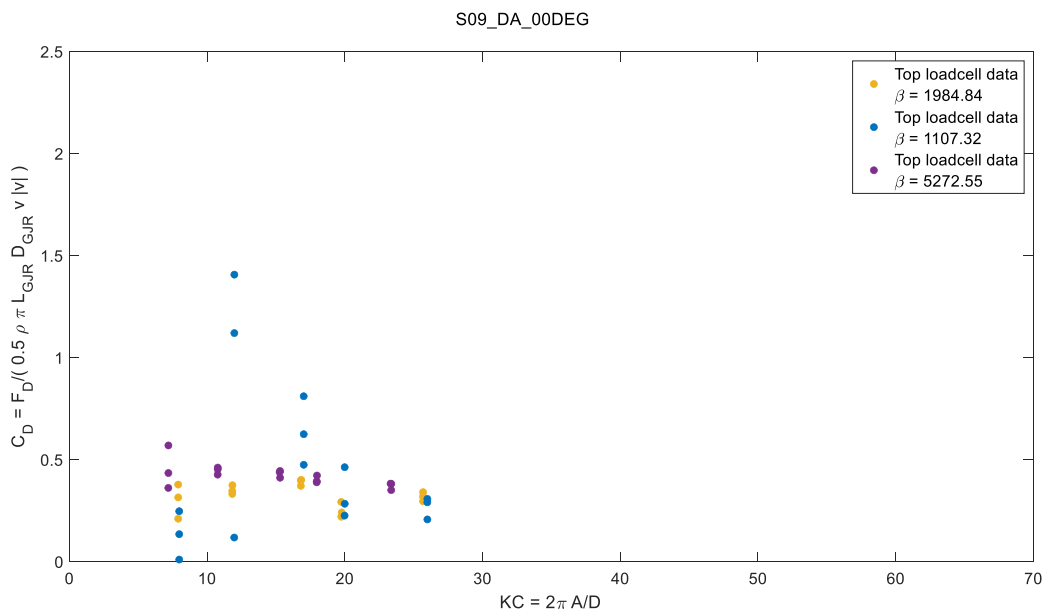


Figure 5-5: Drag coefficient x KC number for the axial oscillation at 1:9 scale at 00DEG

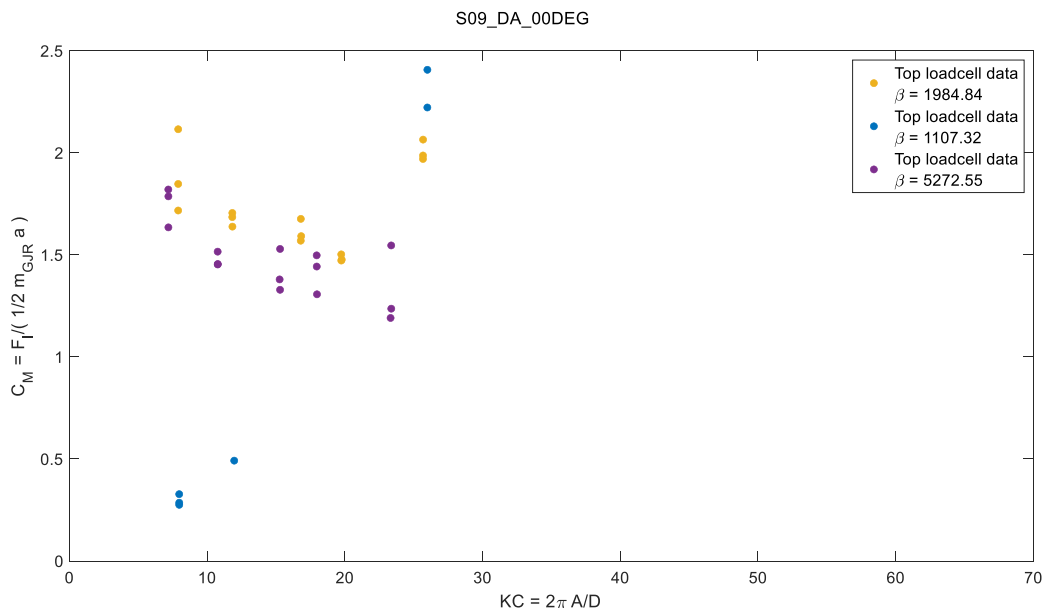


Figure 5-6: Inertia coefficient x KC number for the axial oscillation at 1:9 scale at 00DEG

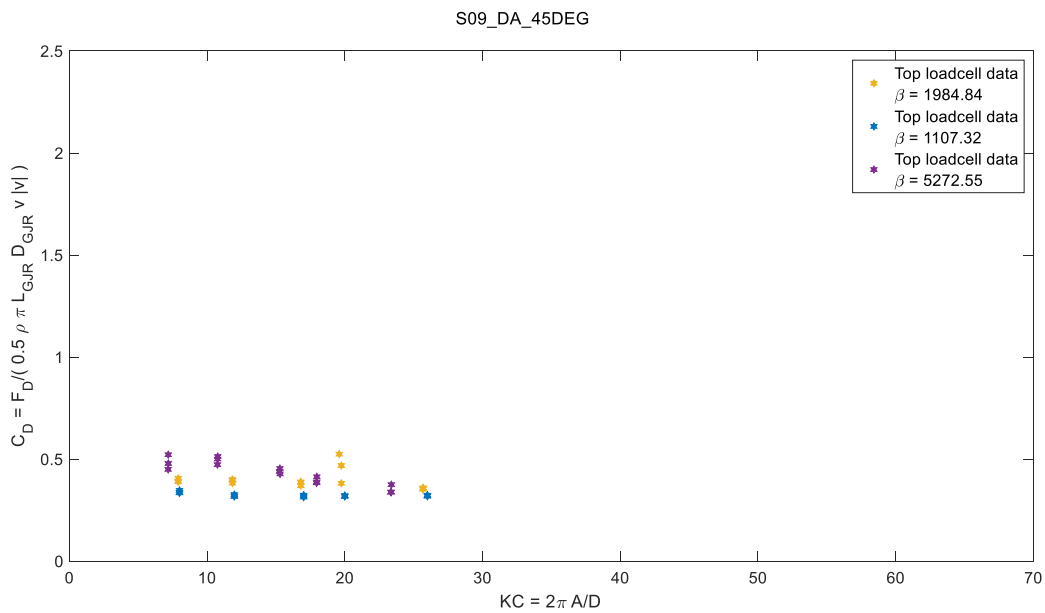


Figure 5-7: Drag coefficient x KC number for the axial oscillation at 1:9 scale at 45DEG

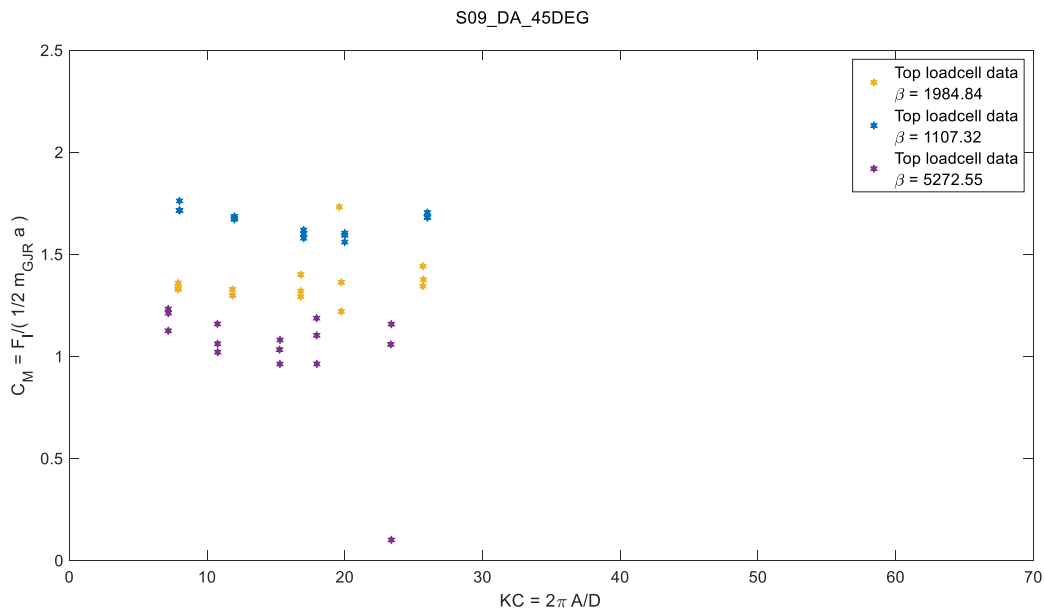


Figure 5-8: Inertia coefficient x KC number for the axial oscillation at 1:9 scale at 45DEG

The hydrodynamic coefficients in the axial oscillation present large dispersion compared to what was observed for the normal oscillation. It is difficult to pin a reason to explain why the dispersion in this configuration is larger than that of the normal oscillation given the repeatability observed (see Appendix A.1). It can be related to hydrodynamic effects due to the non-faired leading and trailing edges of the model, which make the test very sensible to the initial conditions of the fluid.

Table 5-3: Drag coefficient x KC number for the axial oscillation at 1:9 scale at 00DEG and 45DEG

CASE		CD at 00 DEG					CD at 45 DEG				
β	KC	R1 (-)	R2 (-)	R3 (-)	MEAN (-)	ERROR RMS %	R1 (-)	R2 (-)	R3 (-)	MEAN (-)	ERROR RMS %
1984.84	7.91	0.41	0.39	0.39	0.40	1.83%	0.21	0.32	0.38	0.30	22.86%
1107.32	8.00	0.34	0.33	0.35	0.34	1.57%	0.25	0.14	0.01	0.13	73.40%
5272.55	7.18	0.45	0.52	0.48	0.48	6.12%	0.36	0.44	0.57	0.46	18.91%
1984.84	11.85	0.40	0.38	0.40	0.39	1.95%	0.38	0.35	0.33	0.35	5.03%
1107.32	11.99	0.32	0.33	0.32	0.32	1.23%	0.12	1.12	1.41	0.88	62.57%
5272.55	10.76	0.47	0.51	0.50	0.50	3.35%	0.45	0.46	0.43	0.45	3.30%
1984.84	16.81	0.39	0.39	0.37	0.38	2.07%	0.40	0.40	0.37	0.39	3.38%
1107.32	17.02	0.31	0.32	0.32	0.32	1.27%	0.48	0.81	0.63	0.64	21.54%
5272.55	15.29	0.45	0.44	0.43	0.44	2.44%	0.41	0.44	0.45	0.43	3.33%
1984.84	19.60	0.52	0.38	0.47	0.46	12.83%	0.24	0.22	0.29	0.25	12.09%
1107.32	20.00	0.32	0.32	0.32	0.32	0.46%	0.46	0.23	0.28	0.33	31.03%
5272.55	17.96	0.39	0.41	0.38	0.40	3.32%	0.39	0.42	0.39	0.40	3.64%
1984.84	25.68	0.36	0.36	0.35	0.36	0.81%	0.30	0.34	0.32	0.32	5.71%
1107.32	26.00	0.32	0.32	0.32	0.32	0.67%	0.21	0.31	0.29	0.27	16.32%
5272.55	23.38	0.34	0.34	0.37	0.35	4.93%	0.38	0.35	0.38	0.37	3.95%

Table 5-4: Inertia coefficient x KC number for the axial oscillation at 1:9 scale at 00DEG and 45DEG

CASE		CM at 00 DEG					CM at 45 DEG				
β	KC	R1 (-)	R2 (-)	R3 (-)	MEAN (-)	ERROR RMS %	R1 (-)	R2 (-)	R3 (-)	MEAN (-)	ERROR RMS %
1984.84	7.91	1.33	1.34	1.36	1.34	0.99%	2.12	1.85	1.72	1.89	8.75%
1107.32	8.00	1.76	1.71	1.72	1.73	1.26%	0.33	0.28	0.29	0.30	7.61%
5272.55	7.18	1.23	1.12	1.21	1.19	3.90%	1.82	1.79	1.63	1.75	4.62%
1984.84	11.85	1.30	1.33	1.30	1.31	1.02%	1.64	1.71	1.69	1.68	1.67%
1107.32	11.99	1.69	1.67	1.68	1.68	0.35%	0.49	5.00	5.00	3.50	60.77%
5272.55	10.76	1.16	1.02	1.06	1.08	5.37%	1.45	1.46	1.52	1.47	1.97%
1984.84	16.81	1.32	1.29	1.40	1.34	3.43%	1.59	1.57	1.68	1.61	2.86%
1107.32	17.02	1.62	1.60	1.58	1.60	1.02%	4.83	5.00	5.00	4.94	1.59%
5272.55	15.29	0.96	1.03	1.08	1.02	4.73%	1.53	1.38	1.33	1.41	6.01%
1984.84	19.60	1.73	1.36	1.22	1.44	15.02%	1.48	1.47	1.50	1.48	0.89%
1107.32	20.00	1.56	1.60	1.59	1.59	1.17%	3.73	4.01	4.30	4.01	5.76%
5272.55	17.96	1.10	0.96	1.19	1.08	8.53%	1.44	1.31	1.50	1.42	5.66%
1984.84	25.68	1.34	1.37	1.44	1.39	2.94%	1.99	2.06	1.97	2.01	2.06%
1107.32	26.00	1.70	1.68	1.68	1.69	0.66%	3.02	2.41	2.22	2.55	13.42%
5272.55	23.38	1.16	1.06	0.10	0.77	61.78%	1.24	1.55	1.19	1.32	11.92%

5.1.3. Effect of model rotation

This section compares the hydrodynamic coefficient in each condition for both 00DEG and 45DEG by simply overlapping the plots.

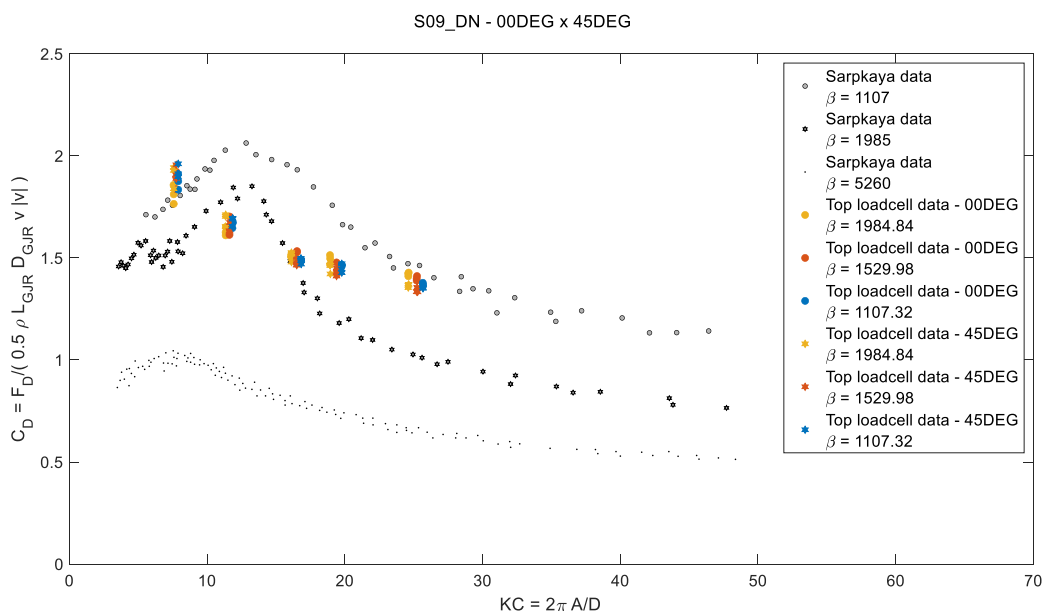


Figure 5-9: Drag coefficient x KC number for the normal oscillation at 1:9 scale – 00DEG x 45DEG

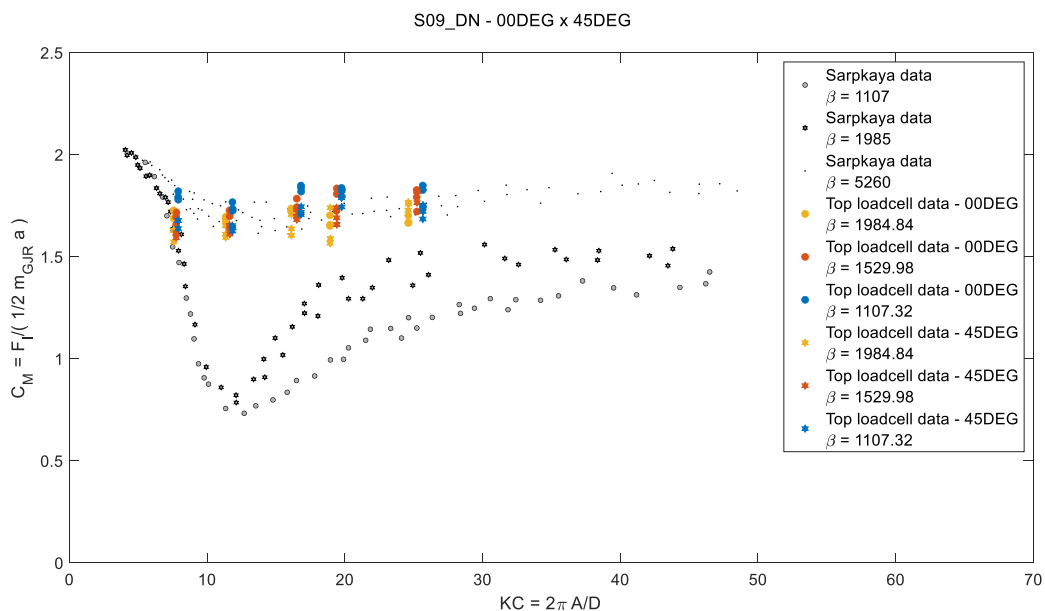


Figure 5-10: Inertia coefficient x KC number for the normal oscillation at 1:9 scale – 00DEG x 45DEG

5.1.4. Effect of model porosity

The following discussed is after client's request [9]. In subsea equipment it is common to assess the hydrodynamic coefficients for ventilated structures. In such situations, it is common to refer to the ratio between void and material volume within the structure as *porosity*, despite not being semantically suitable, and the oscillation amplitude is usually referred to as a ‘*porous KC number*’, as in (5.1), where A is the amplitude of motion, D_{GJR} is the GJR diameter, p is the perforation ratio and μ is nondimensional discharge coefficient [10].

$$KC_{por} = \frac{A}{D_{GJR}} \frac{(1-p)}{2\mu p^2} \quad (5.1)$$

The guidelines in [10] deal with slamming, hence the porosity in the reference is defined in terms of the ratio of the surface area over the projected area of the subsea structure. However, in the present analysis, the porosity p is defined as the ratio of volume between the body over the corresponding cylinder with the same dimensions. Based on the geometry, the porosity for the 1:9 model is $p = 0.341$. The discharge coefficient is taken as 0.9 [9].

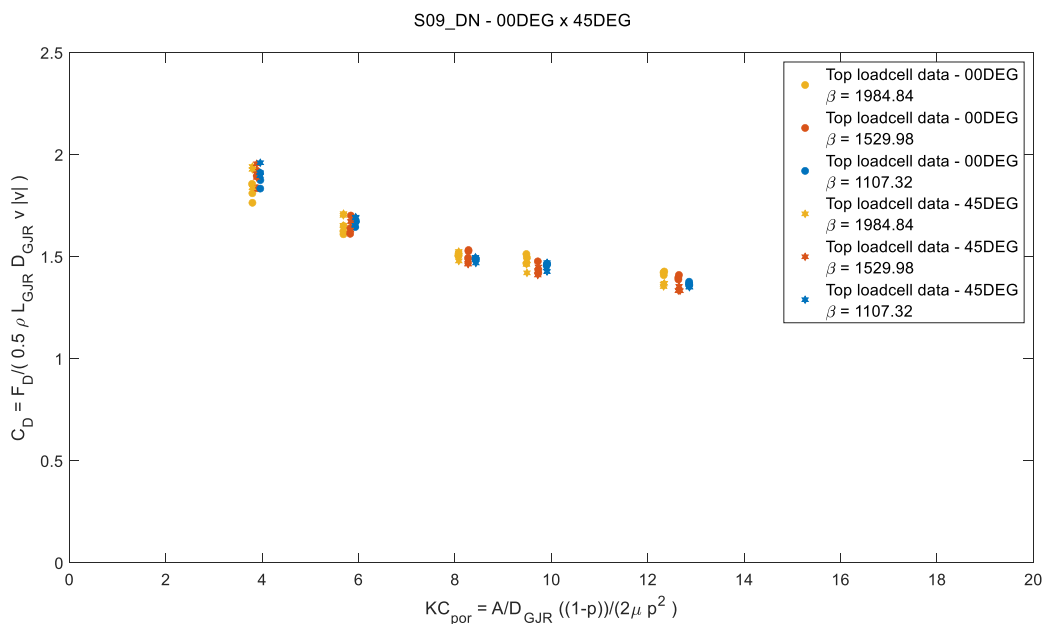


Figure 5-11: Drag coefficient x KC_{por} number for the axial oscillation at 1:9 scale – 00DEG x 45DEG

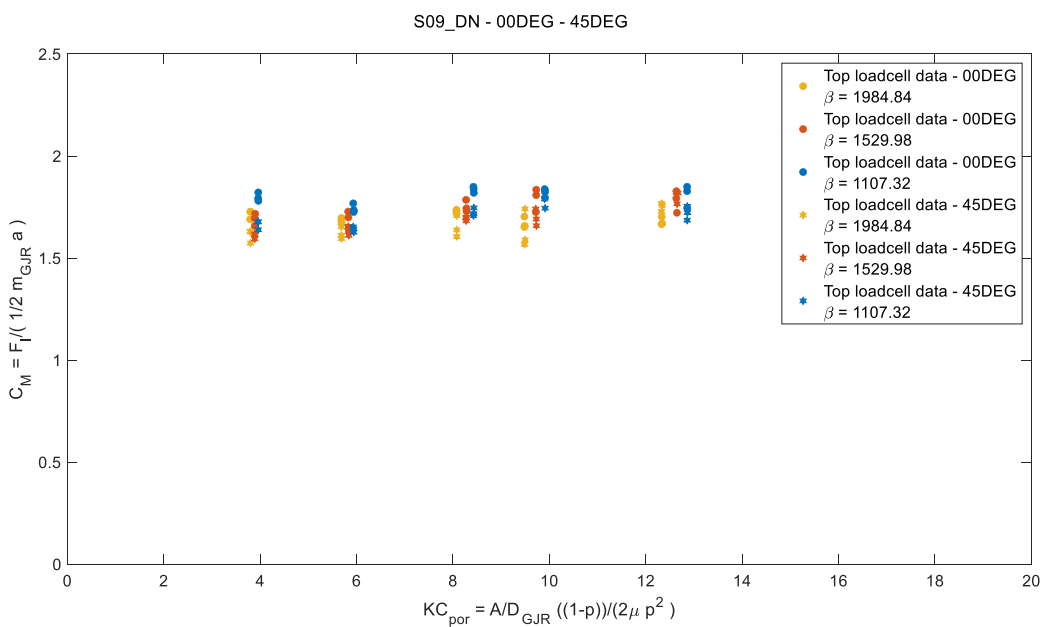


Figure 5-12: Inertia coefficient x KC_{por} number for the axial oscillation at 1:9 scale – 00DEG x 45DEG

5.2.1:30 scale

5.2.1. Normal oscillation at 1:30 scale

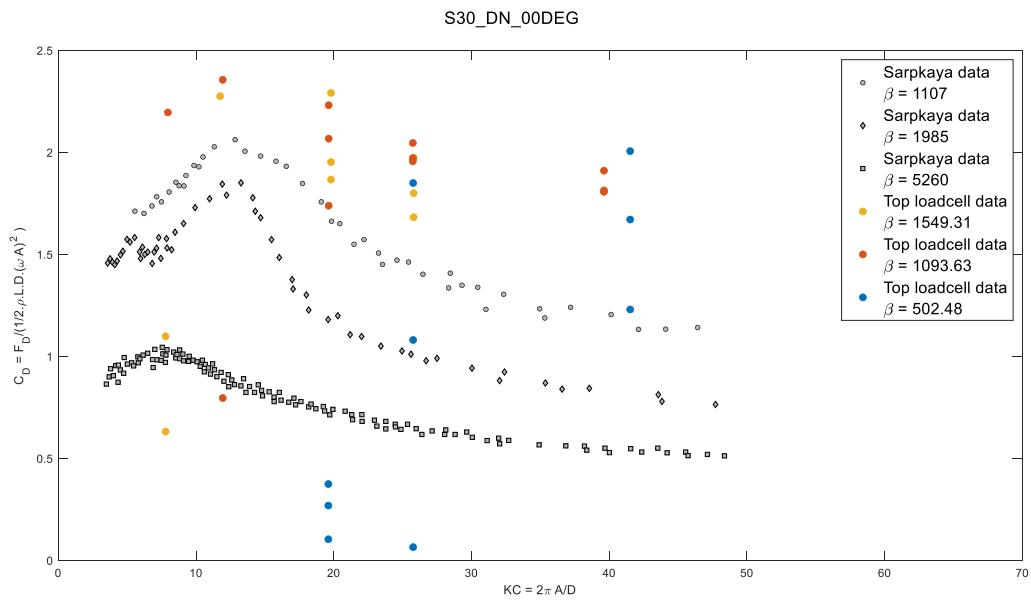


Figure 5-13: Drag coefficient x KC number for the normal oscillation at 1:30 scale at 00DEG at the second run

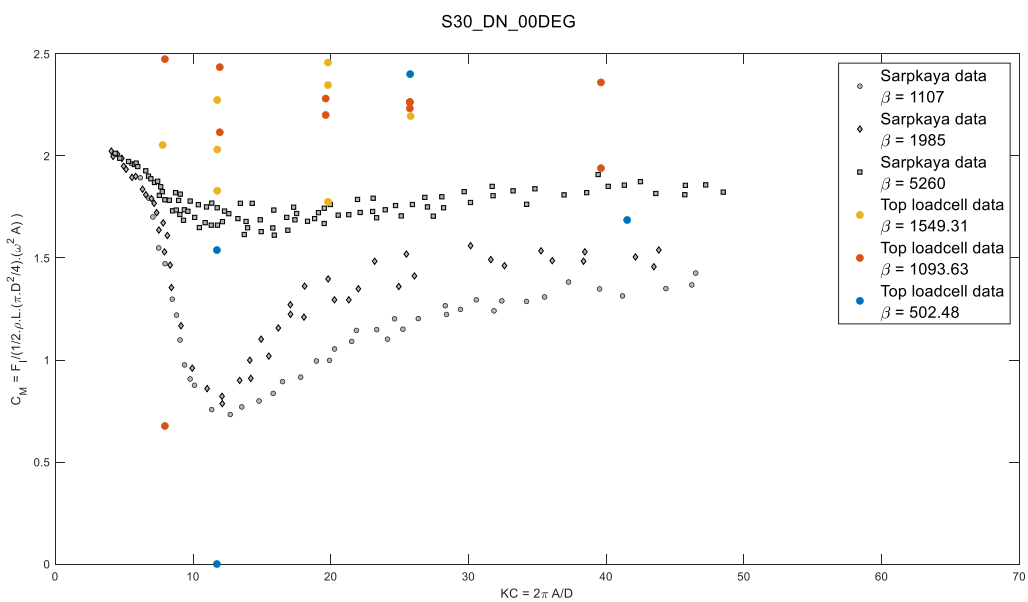


Figure 5-14: Inertia coefficient x KC number for the normal oscillation at 1:30 scale at 00DEG at the second run

Opposed to what was observed for the 1:9 scale, the plots above show a large dispersion of the data and no clear and identifiable trend. The reason for that is still unclear since the time series showed a good repeatability as displayed in Appendix A.

Table 5-5: Drag coefficient x KC number for the normal oscillation at 1:30 scale at 00DEG and 45DEG

CASE		CD at 00 DEG					CD at 45 DEG				
β	KC	R1 (-)	R2 (-)	R3 (-)	MEAN (-)	ERROR RMS %	R1 (-)	R2 (-)	R3 (-)	MEAN (-)	ERROR RMS %
1549.31	19.80	1.95	1.87	2.29	2.04	8.99%	1.33	1.97	1.81	1.70	16.00%
1093.63	19.63	2.23	2.07	1.74	2.01	10.18%	2.00	1.55	1.83	1.79	10.37%
502.48	19.61	0.27	0.37	0.10	0.25	44.64%	1.12	2.12	2.05	1.76	25.93%
1549.31	25.80	1.68	1.97	1.80	1.82	6.58%	1.79	1.62	1.61	1.67	4.92%
1093.63	25.74	2.05	1.97	1.96	1.99	1.97%	1.33	1.43	1.08	1.28	11.40%
502.48	25.77	1.85	1.08	0.07	1.00	73.14%	1.20	1.47	0.96	1.21	17.27%
-	-	-	-	-	-	-	-	-	-	-	-
1093.63	39.62	1.91	1.81	1.81	1.84	2.56%	0.89	0.87	0.82	0.86	3.19%
502.48	41.53	1.23	2.01	1.67	1.64	19.42%	1.51	1.39	1.54	1.48	4.26%
1549.31	7.80	3.37	1.10	0.63	1.70	70.37%	2.78	4.22	2.61	3.20	22.50%
1093.63	7.96	-2.00	5.00	2.20	1.73	166.07%	-1.48	-2.00	-0.39	-1.29	-51.82%
502.48	7.87	-2.00	4.85	5.00	2.62	124.76%	2.39	1.28	3.93	2.53	42.93%
1549.31	11.76	2.53	2.67	2.28	2.49	6.56%	1.15	1.60	2.18	1.65	25.56%
1093.63	11.94	2.55	0.80	2.36	1.90	41.33%	1.56	1.56	1.79	1.64	6.56%
502.48	11.73	4.96	5.00	5.00	4.99	0.40%	0.11	4.28	1.85	2.08	82.39%

Table 5-6: Inertia coefficient x KC number for the normal oscillation at 1:30 scale at 00DEG and 45DEG

CASE		CM at 00 DEG					CM at 45 DEG				
β	KC	R1 (-)	R2 (-)	R3 (-)	MEAN (-)	ERROR RMS %	R1 (-)	R2 (-)	R3 (-)	MEAN (-)	ERROR RMS %
1549.31	19.80	2.35	2.46	1.78	2.19	13.63%	2.07	1.42	1.64	1.71	16.02%
1093.63	19.63	2.20	2.28	2.59	2.36	7.17%	1.12	1.80	1.57	1.49	18.91%
502.48	19.61	4.87	4.85	4.26	4.66	6.05%	2.59	0.79	1.67	1.69	43.61%
1549.31	25.80	2.79	2.20	2.53	2.50	9.67%	1.85	1.53	1.40	1.60	11.81%
1093.63	25.74	2.23	2.26	2.26	2.25	0.64%	2.03	1.97	2.48	2.16	10.63%
502.48	25.77	2.40	4.06	5.00	3.82	28.12%	2.59	1.44	2.99	2.34	28.08%
-	-	-	-	-	-	-	-	-	-	-	-
1093.63	39.62	1.94	2.56	2.36	2.29	11.29%	0.00	0.00	0.00	0.00	1.64%
502.48	41.53	5.00	1.69	3.06	3.25	41.84%	1.14	1.60	1.62	1.45	15.24%
1549.31	7.80	2.05	2.58	2.70	2.44	11.49%	1.66	1.18	1.80	1.55	17.08%
1093.63	7.96	3.84	0.68	2.47	2.33	55.55%	2.42	3.50	2.92	2.95	14.97%
502.48	7.87	5.00	3.11	4.06	4.05	19.08%	1.31	2.32	1.05	1.56	34.99%
1549.31	11.76	2.03	1.83	2.27	2.05	8.89%	2.18	1.91	1.69	1.93	10.35%
1093.63	11.94	2.12	2.95	2.44	2.50	13.71%	1.85	1.96	1.77	1.86	4.17%
502.48	11.73	1.54	5.00	0.00	2.18	95.94%	2.75	0.00	1.73	1.49	76.07%

5.2.2. Axial oscillation at 1:30 scale

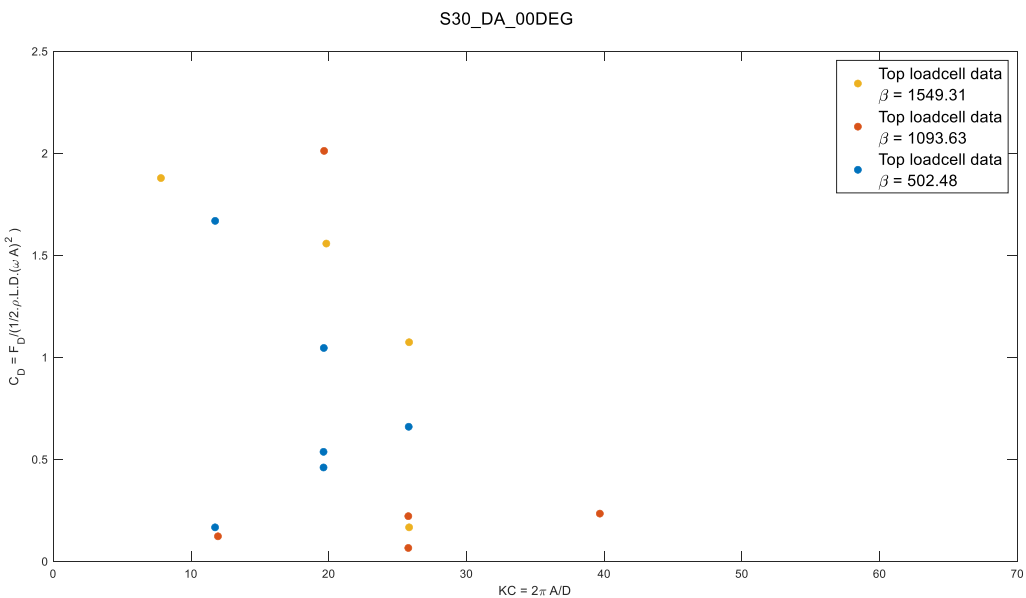


Figure 5-15: Drag coefficient x KC number for the axial oscillation at 1:30 scale at 00DEG at the second run

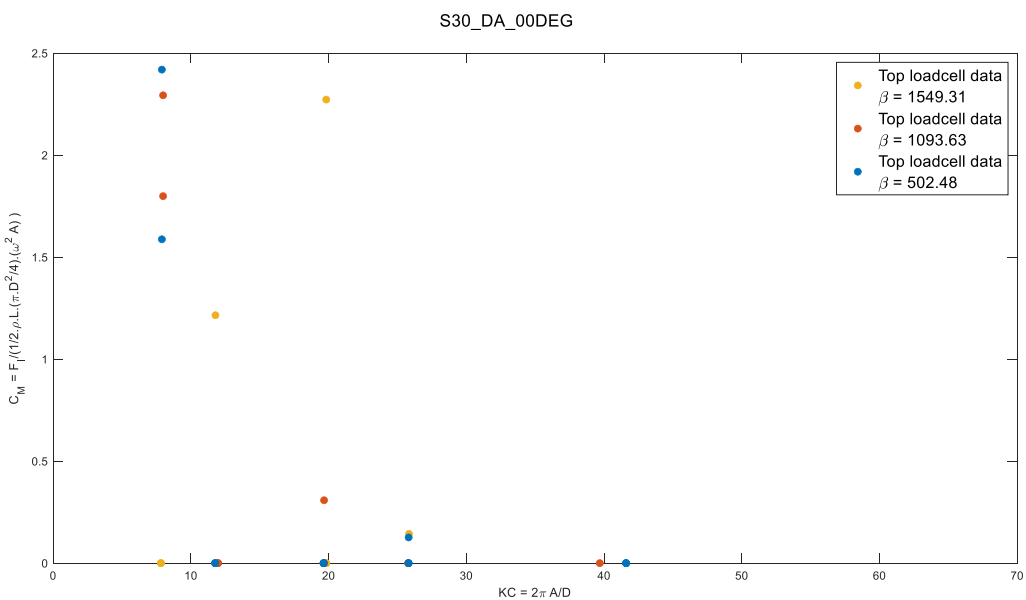


Figure 5-16: Inertia coefficient x KC number for the axial oscillation at 1:30 scale at 00DEG at the second run

In the axial oscillation at 1:30 the data also show large dispersion observed for the normal excitation. Cases in which one of the coefficients are null happened due to the limits set for the least-square adjustment.

Table 5-7: Drag coefficient x KC number for the axial oscillation at 1:30 scale at 00DEG and 45DEG

CASE		CD at 00 DEG					CD at 45 DEG				
β	KC	R1 (-)	R2 (-)	R3 (-)	MEAN (-)	ERROR RMS %	R1 (-)	R2 (-)	R3 (-)	MEAN (-)	ERROR RMS %
1549.31	19.82	-2.00	1.56	-2.00	-0.81	-205.94%	-0.57	-0.83	1.43	0.01	12476.34%
1093.63	19.66	-1.59	-1.32	2.01	-0.30	-544.75%	0.71	0.40	-0.04	0.36	86.43%
502.48	19.62	0.54	0.46	1.05	0.68	38.19%	-1.57	0.71	-0.09	-0.32	-299.98%
1549.31	25.84	1.07	-1.42	0.17	-0.06	1718.73%	0.75	0.05	0.73	0.51	64.25%
1093.63	25.78	0.22	-0.19	0.07	0.03	546.92%	-0.07	-0.22	0.50	0.07	435.39%
502.48	25.81	-1.06	0.66	-0.50	-0.30	-237.59%	-0.05	-0.56	0.62	0.00	11840.98%
-	-	-	-	-	-	-	-	-	-	-	-
1093.63	39.69	-0.31	-0.22	0.23	-0.10	-243.57%	0.06	-1.32	0.02	-0.41	-155.44%
502.48	41.60	-0.07	-0.25	-0.35	-0.22	-52.33%	0.32	0.51	-0.82	0.00	16950.88%
1549.31	7.82	-2.00	1.88	-2.00	-0.71	-258.50%	1.52	-2.00	1.02	0.18	856.53%
1093.63	7.97	-2.00	-2.00	-2.00	-2.00	0.00%	0.28	1.30	-0.17	0.47	132.00%
502.48	7.89	-2.00	-2.00	-1.47	-1.82	-13.60%	0.20	3.04	-0.68	0.85	185.74%
1549.31	11.78	3.60	-1.14	-1.44	0.34	677.04%	-1.03	1.95	3.03	1.32	130.48%
1093.63	11.96	-0.67	-0.02	0.12	-0.19	-180.64%	0.01	0.62	0.87	0.50	72.30%
502.48	11.75	1.67	0.17	2.90	1.58	70.86%	2.61	0.84	1.00	1.48	53.86%

Table 5-8: Inertia coefficient x KC number for the axial oscillation at 1:30 scale at 00DEG and 45DEG

CASE		CM at 00 DEG					CM at 45 DEG				
β	KC	R1 (-)	R2 (-)	R3 (-)	MEAN (-)	ERROR RMS %	R1 (-)	R2 (-)	R3 (-)	MEAN (-)	ERROR RMS %
1549.31	19.82	2.27	0.00	0.00	0.76	141.42%	0.00	0.00	0.87	0.29	141.42%
1093.63	19.66	0.00	0.00	0.31	0.10	141.42%	0.00	0.00	0.00	0.00	75.77%
502.48	19.62	0.00	0.00	0.00	0.00	99.89%	0.00	0.50	0.00	0.17	141.42%
1549.31	25.84	3.94	0.14	5.00	3.03	68.86%	0.12	0.00	0.42	0.18	99.03%
1093.63	25.78	0.00	0.00	0.00	0.00	141.39%	0.00	0.00	1.85	0.62	141.42%
502.48	25.81	0.00	0.13	0.00	0.04	141.42%	0.00	0.00	0.39	0.13	141.42%
-	-	-	-	-	-	-	-	-	-	-	-
1093.63	39.69	5.00	5.00	0.00	3.33	70.71%	2.69	1.28	3.16	2.38	33.63%
502.48	41.60	0.00	0.00	0.00	0.00	77.42%	0.00	0.36	0.00	0.12	141.42%
1549.31	7.82	0.00	0.00	3.73	1.24	141.42%	0.71	0.00	0.09	0.27	117.82%
1093.63	7.97	2.29	1.80	2.62	2.24	15.13%	0.00	0.15	0.00	0.05	141.42%
502.48	7.89	2.42	1.59	5.00	3.00	48.39%	1.76	1.18	0.00	0.98	74.69%
1549.31	11.78	1.22	0.00	0.00	0.41	141.42%	0.00	0.00	1.01	0.34	141.42%
1093.63	11.96	0.00	0.00	0.00	0.00	89.70%	0.00	0.00	0.00	0.00	59.29%
502.48	11.75	0.00	0.00	3.33	1.11	141.42%	3.64	1.12	1.03	1.93	62.69%

5.2.3. Effect of model porosity

As in section 5.1.4, the hydrodynamic coefficients were plotted against the porous KC number (5.1).

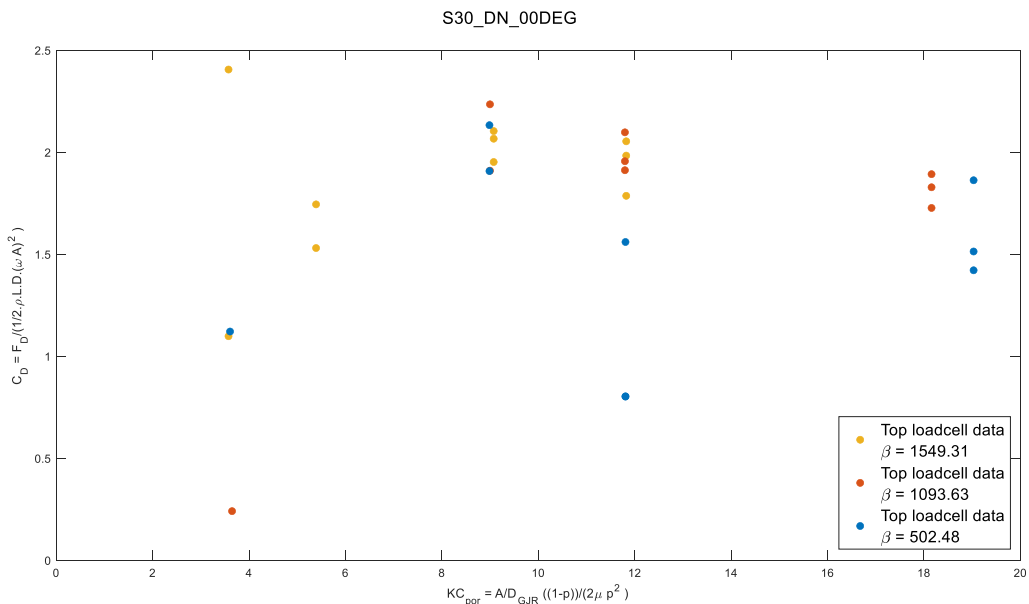


Figure 5-17: Drag coefficient x KC_{por} number for the axial oscillation at 1:30 scale – 00DEG

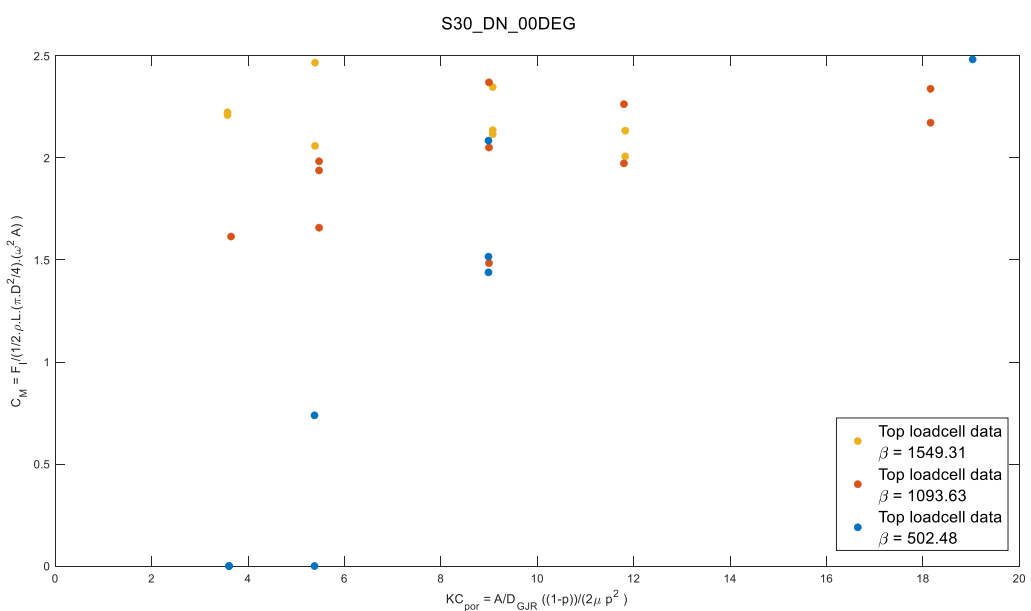


Figure 5-18: Inertia coefficient x KC_{por} number for the axial oscillation at 1:30 scale – 00DEG

5.3.Final comments on the results

The sections above present the hydrodynamic coefficients of the GJR model in two different scales in different configurations and submitted to broad range of oscillations (periods and amplitudes).

The data for drag and inertia coefficients for the normal oscillation at 1:9 scale present a clear behavior, apparently independent of the Reynolds number. The axial excitation presented larger dispersion compared to the normal oscillation. Both drag and inertia coefficients seem to depend on the Reynolds number, and besides a couple of outliers the points spread in clear trends.

The tests at 1:30 scale, however, the dispersion of the points is even larger, despite the good repeatability observed for the motion and loads in Appendix A. The reason for such dispersion is still unclear to the point that it is not advisable to make any conjecture on scale effects. This leads to suggestions for future research.

Despite unclear from the 1:30 tests, it seems appropriate to expect hydrodynamic coefficients in the same order of magnitude of a smooth cylinder. Other effects, which were not investigated in this piece study, could be further explored in future research, such as the behavior of the flow within the GJR and its effects on the TCP, which could be done by using Flow Visualization tools like a PIV (*Particle Image Velocimeter*) or even numerical studies with CFD (*Computational Fluid Dynamics*). The independency of CD and CM to the Reynolds number could also be investigated using similar tools to visualize the pattern of vortex shedding.

6. References

- [1] LOC, "SS7_21_02-TRF_01_D - Test Request Form for Hydrodynamic model tests of 1:9 Gimbal Joint Riser (GJR)".
- [2] LOC, "SS7_21_02-TRF_02_D - Test Request Form for Hydrodynamic model tests of 1:30 Gimbal Joint Riser (GJR)," 2022.
- [3] LOC, "SS7_21_02-TPR_001_B - Test Procedures of forced oscillation of Gimbal Joint Riser".
- [4] LOC, SS7_21_02-ESR_001_D - Experimental Setup Report for Hydrodynamic Tests of GJR in LOC, 2022.
- [5] LOC, SS7_21_02-MTR_001_B - Model Test Report for Hydrodynamic Tests of GJR in LOC, 2022.
- [6] LOC, "PMS_GIH_002_21_001.1 - Premises LOC hydrodynamic test".
- [7] ITTC: Quality System Group of the 28th International Towing Tank, "7.5-02-01-03: Fresh water and seawater properties," in *ITTC Recommended Procedures and Guidelines*, 2011.
- [8] T. Sarpkaya, "Forces on Cylinders and Spheres in a Sinusoidally Oscillating Fluid," *Journal of Applied Mechanics*, 1975.
- [9] Subsea7 representative, "Online meet," 07/25/2022.
- [10] DNVGL-RP-N103, "Modelling and analysis of marine operations," 2017.
- [11] D. Costa, "Scaled model test specification for Gimbal Joint Riser - hydrodynamic tests_v1," 2021.
- [12] O. E. C. o. t. 2. I. T. T. C. ITTC, "7.5-01-03-01: Uncertainty analysis, instrument calibration," in *ITTC Recommended Procedures and Guidelines*, 2017.

Appendix A. Repeatability analysis

A.1. Axial oscillations at 1:9 scale

The repeatability check was carried out by calculating the equivalent harmonic amplitude (3.1) for each run, as compiled and displayed in for the amplitude of motion (vertical gray bars) and for the amplitude of loads (blue curve). Each 3 consecutive point represents the 3 repetitions for each case, and the figure below a good match of the amplitudes of each case. The data corresponding to Figure A-1 is presented in Table A-1. It is noticeable how some cases present larger variation on the load amplitude, as highlighted in Table A-2, which is not observed for the amplitude of motion.

The same analysis was carried out for the model rotated by 45 degrees around itself, as summarized in Figure A-2 and Table A-2.

The repeatability check for the oscillation of the structure alone is illustrated by Figure A-3.

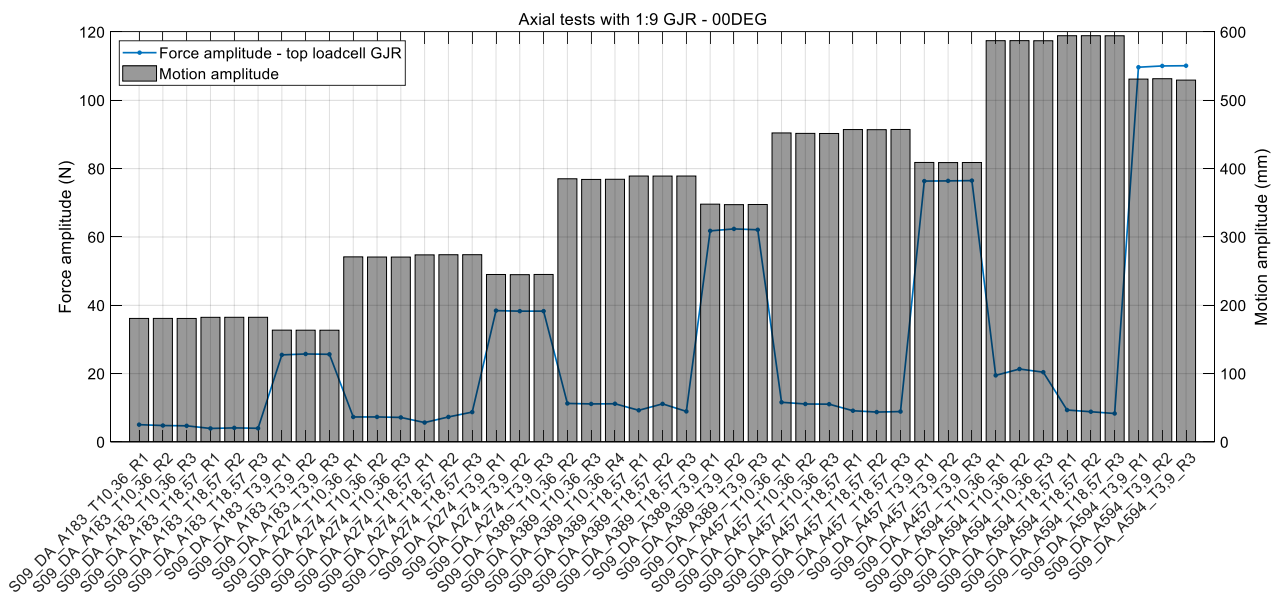


Figure A-1: Amplitudes of motion (bars) and load (blue curve) in each run – repeatability check for axial oscillations at 00DEG at 1:9 scale

Table A-1: Repeatability check for 1:9 axial oscillations at 00DEG

CASE	AMPLITUDE OF MOTION					AMPLITUDE OF LOAD				
	R1 (mm)	R2 (mm)	R3 (mm)	MEAN (mm)	ERROR RMS %	R1 (N)	R2 (N)	R3 (N)	MEAN (N)	ERROR RMS %
S09_DA_00DEG_A183_T18,57	182.42	182.46	182.46	182.45	0.01%	3.96	4.12	4.01	4.03	1.74%
S09_DA_00DEG_A274_T18,57	273.82	274.04	274.08	273.98	0.04%	5.69	7.33	8.75	7.25	17.26%
S09_DA_00DEG_A389_T18,57	389.21	389.16	389.21	389.19	0.01%	9.27	11.15	8.95	9.79	9.94%
S09_DA_00DEG_A457_T18,57	457.24	457.05	457.35	457.21	0.03%	9.14	8.75	8.90	8.93	1.81%
S09_DA_00DEG_A594_T18,57	594.55	594.57	594.49	594.54	0.01%	9.35	8.85	8.34	8.84	4.68%
S09_DA_00DEG_A183_T10,36	180.81	180.84	180.77	180.81	0.02%	5.07	4.81	4.73	4.87	2.96%
S09_DA_00DEG_A274_T10,36	270.90	270.68	270.61	270.73	0.05%	7.32	7.33	7.18	7.28	0.92%
S09_DA_00DEG_A389_T10,36	385.18	384.24	384.45	384.63	0.11%	11.28	11.14	11.19	11.20	0.53%
S09_DA_00DEG_A457_T10,36	452.27	451.62	451.47	451.79	0.08%	11.62	11.12	11.07	11.27	2.20%
S09_DA_00DEG_A594_T10,36	587.31	587.36	587.20	587.29	0.01%	19.49	21.36	20.42	20.42	3.74%
S09_DA_00DEG_A183_T3,9	163.68	163.59	163.56	163.61	0.03%	25.49	25.76	25.66	25.64	0.44%
S09_DA_00DEG_A274_T3,9	245.11	244.86	245.15	245.04	0.05%	38.44	38.29	38.30	38.34	0.18%
S09_DA_00DEG_A389_T3,9	348.04	347.33	347.54	347.64	0.09%	61.79	62.37	62.11	62.09	0.38%
S09_DA_00DEG_A457_T3,9	409.08	408.89	408.99	408.99	0.02%	76.36	76.42	76.50	76.43	0.08%
S09_DA_00DEG_A594_T3,9	531.06	531.63	529.61	530.77	0.16%	109.69	110.06	110.13	109.96	0.18%

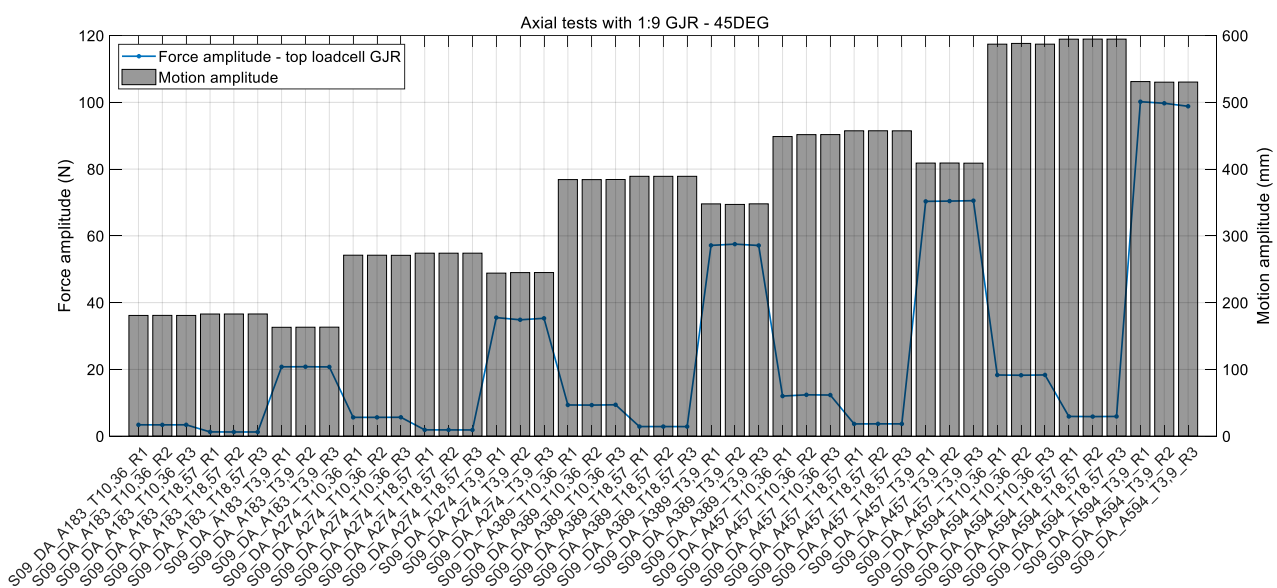


Figure A-2: Amplitudes of motion (bars) and load (blue curve) in each run – repeatability check for axial oscillations at 45DEG at 1:9 scale

Table A-2: Repeatability check for 1:9 axial oscillations at 45DEG

CASE	AMPLITUDE OF MOTION					AMPLITUDE OF LOAD				
	R1 (mm)	R2 (mm)	R3 (mm)	MEAN (mm)	ERROR RMS %	R1 (N)	R2 (N)	R3 (N)	MEAN (N)	ERROR RMS %
S09_DA_45DEG_A183_T18,57	182.95	182.99	183.02	182.99	0.01%	1.28	1.26	1.26	1.26	0.69%
S09_DA_45DEG_A274_T18,57	274.08	274.06	274.08	274.07	0.00%	1.89	1.88	1.87	1.88	0.49%
S09_DA_45DEG_A389_T18,57	389.20	389.17	389.18	389.18	0.00%	2.88	2.88	2.87	2.88	0.21%
S09_DA_45DEG_A457_T18,57	457.36	457.38	457.31	457.35	0.01%	3.67	3.69	3.69	3.68	0.26%
S09_DA_45DEG_A594_T18,57	594.57	594.67	594.63	594.62	0.01%	5.91	5.86	5.91	5.90	0.39%
S09_DA_45DEG_A183_T10,36	180.82	180.91	180.83	180.85	0.02%	3.41	3.39	3.41	3.40	0.26%
S09_DA_45DEG_A274_T10,36	271.04	271.02	270.86	270.97	0.03%	5.64	5.63	5.66	5.64	0.19%
S09_DA_45DEG_A389_T10,36	384.29	384.26	384.41	384.32	0.02%	9.34	9.31	9.41	9.35	0.43%
S09_DA_45DEG_A457_T10,36	448.77	451.63	451.69	450.69	0.30%	12.01	12.39	12.32	12.24	1.35%
S09_DA_45DEG_A594_T10,36	587.10	588.21	587.12	587.48	0.09%	18.33	18.25	18.35	18.31	0.23%
S09_DA_45DEG_A183_T3,9	163.07	163.19	163.28	163.18	0.05%	20.77	20.81	20.75	20.78	0.12%
S09_DA_45DEG_A274_T3,9	244.20	244.99	245.08	244.76	0.16%	35.52	34.86	35.31	35.23	0.78%
S09_DA_45DEG_A389_T3,9	347.89	347.09	347.97	347.65	0.11%	57.15	57.53	57.12	57.26	0.32%
S09_DA_45DEG_A457_T3,9	409.02	409.09	408.89	409.00	0.02%	70.33	70.42	70.54	70.43	0.12%
S09_DA_45DEG_A594_T3,9	531.08	530.19	530.36	530.54	0.07%	100.18	99.71	98.82	99.57	0.57%

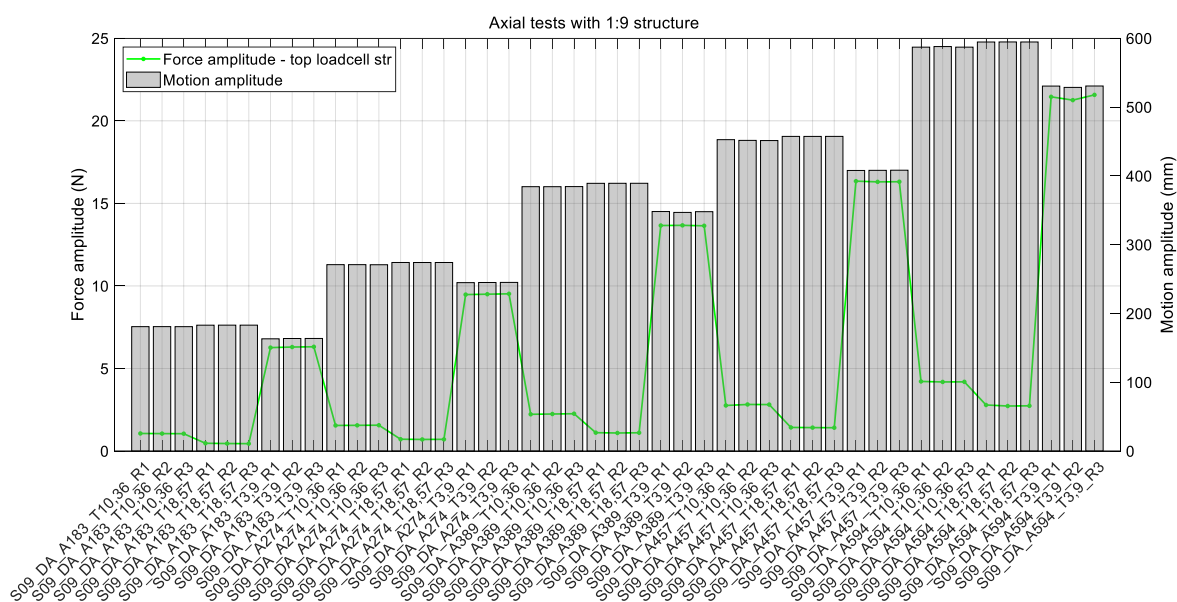


Figure A-3: Amplitudes of motion (bars) and load (blue curve) in each run – repeatability check for axial oscillations of the structure at 1:9 scale

A.2. Normal oscillations at 1:9 scale

The repeatability check is illustrated by the figures below for both the amplitudes of motion (gray bars) and load (blue curve), showing the ergodicity of the test runs, corresponding again at the data displayed in tables below.

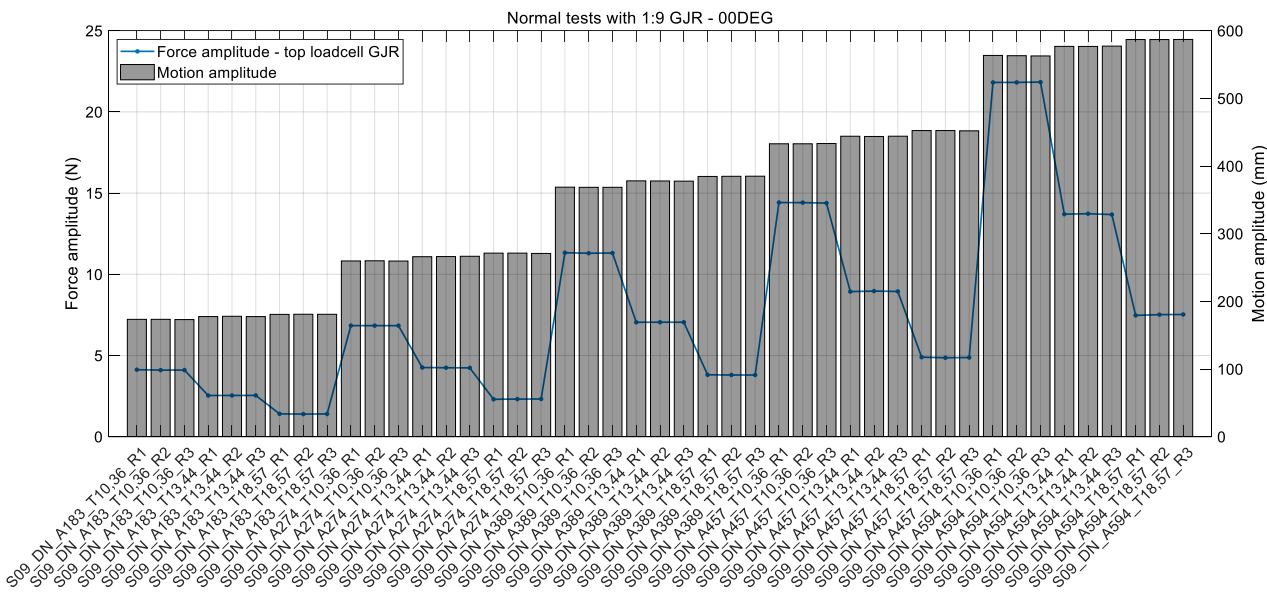


Figure A-4: Amplitudes of motion (bars) and load (blue curve) in each run – repeatability check for normal oscillations at 00DEG at 1:9 scale

Table A-3: Repeatability check for 1:9 normal oscillations at 00DEG

CASE	AMPLITUDE OF MOTION					AMPLITUDE OF LOAD				
	R1 (mm)	R2 (mm)	R3 (mm)	MEAN (mm)	ERROR RMS %	R1 (N)	R2 (N)	R3 (N)	MEAN (N)	ERROR RMS %
S09_DN_00DEG_A183_T18,57	180.75	180.93	180.86	180.85	0.04%	1.41	1.39	1.40	1.40	0.45%
S09_DN_00DEG_A274_T18,57	271.27	271.28	270.79	271.11	0.08%	2.30	2.31	2.32	2.31	0.34%
S09_DN_00DEG_A389_T18,57	384.60	384.81	384.95	384.79	0.04%	3.81	3.80	3.80	3.80	0.17%
S09_DN_00DEG_A457_T18,57	452.41	452.41	452.02	452.28	0.04%	4.90	4.86	4.87	4.88	0.29%
S09_DN_00DEG_A594_T18,57	586.93	586.91	587.06	586.97	0.01%	7.47	7.51	7.53	7.50	0.33%
S09_DN_00DEG_A183_T13,44	177.50	177.94	177.48	177.64	0.12%	2.54	2.54	2.54	2.54	0.09%
S09_DN_00DEG_A274_T13,44	265.99	266.19	266.60	266.26	0.10%	4.26	4.25	4.24	4.25	0.21%
S09_DN_00DEG_A389_T13,44	378.05	377.90	377.66	377.87	0.04%	7.04	7.05	7.05	7.05	0.02%
S09_DN_00DEG_A457_T13,44	444.02	443.68	444.06	443.92	0.04%	8.93	8.97	8.94	8.95	0.16%
S09_DN_00DEG_A594_T13,44	576.80	576.75	577.21	576.92	0.04%	13.70	13.73	13.68	13.70	0.16%
S09_DN_00DEG_A183_T10,36	173.39	173.42	173.07	173.29	0.09%	4.12	4.10	4.10	4.11	0.28%
S09_DN_00DEG_A274_T10,36	259.70	259.93	259.55	259.72	0.06%	6.84	6.84	6.84	6.84	0.02%
S09_DN_00DEG_A389_T10,36	368.74	368.51	368.53	368.59	0.03%	11.33	11.30	11.31	11.31	0.11%
S09_DN_00DEG_A457_T10,36	432.85	432.87	433.26	432.99	0.04%	14.42	14.41	14.38	14.41	0.11%
S09_DN_00DEG_A594_T10,36	563.45	563.05	562.69	563.06	0.05%	21.81	21.82	21.83	21.82	0.04%

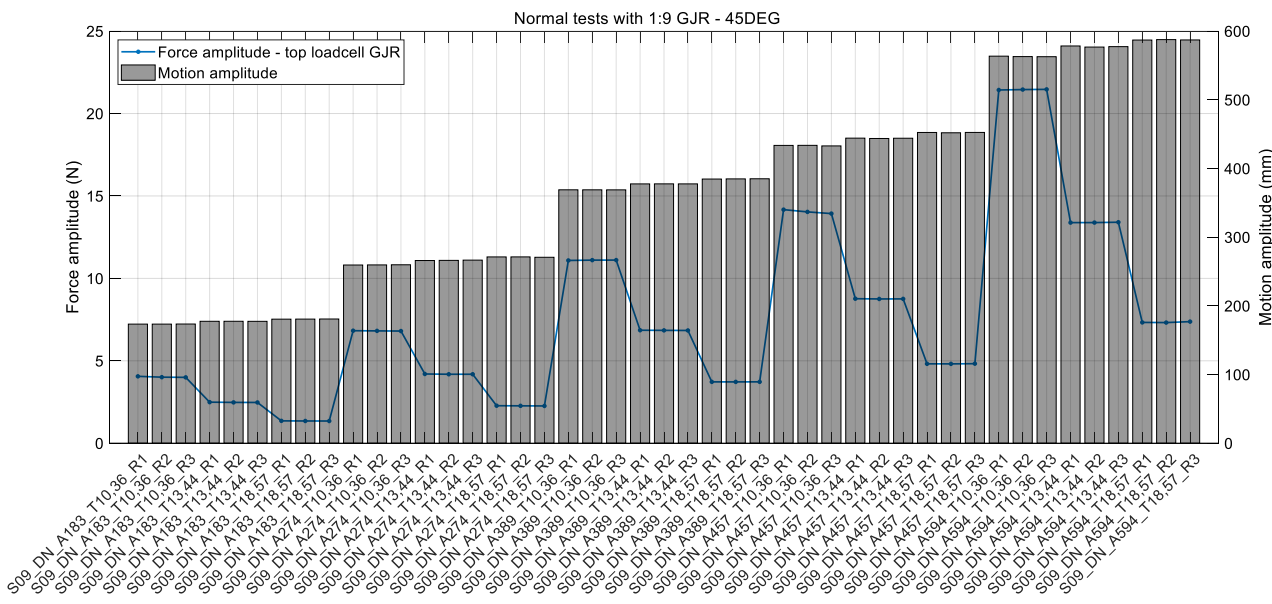


Figure A-5: Amplitudes of motion (bars) and load (blue curve) in each run – repeatability check for normal oscillations at 45DEG at 1:9 scale

Table A-4: Repeatability check for 1:9 normal oscillations at 45DEG

CASE	AMPLITUDE OF MOTION					AMPLITUDE OF LOAD				
	R1 (mm)	R2 (mm)	R3 (mm)	MEAN (mm)	ERROR RMS %	R1 (N)	R2 (N)	R3 (N)	MEAN (N)	ERROR RMS %
S09_DN_45DEG_A183_T18,57	180.62	180.70	180.85	180.72	0.05%	1.36	1.35	1.35	1.35	0.29%
S09_DN_45DEG_A274_T18,57	271.24	271.27	270.71	271.07	0.10%	2.27	2.27	2.26	2.27	0.26%
S09_DN_45DEG_A389_T18,57	384.62	384.84	385.02	384.83	0.04%	3.72	3.72	3.72	3.72	0.04%
S09_DN_45DEG_A457_T18,57	452.42	451.96	452.48	452.29	0.05%	4.82	4.81	4.83	4.82	0.11%
S09_DN_45DEG_A594_T18,57	587.00	587.62	587.13	587.25	0.05%	7.33	7.32	7.38	7.34	0.34%
S09_DN_45DEG_A183_T13,44	177.50	177.55	177.46	177.51	0.02%	2.49	2.48	2.47	2.48	0.33%
S09_DN_45DEG_A274_T13,44	265.98	266.20	266.58	266.25	0.09%	4.20	4.18	4.18	4.19	0.19%
S09_DN_45DEG_A389_T13,44	377.53	377.59	377.55	377.56	0.01%	6.85	6.85	6.84	6.85	0.08%
S09_DN_45DEG_A457_T13,44	444.17	443.68	444.04	443.96	0.05%	8.77	8.75	8.76	8.76	0.08%
S09_DN_45DEG_A594_T13,44	578.35	576.77	577.39	577.50	0.11%	13.38	13.38	13.41	13.39	0.08%
S09_DN_45DEG_A183_T10,36	173.42	173.42	173.53	173.46	0.03%	4.06	4.01	3.99	4.02	0.67%
S09_DN_45DEG_A274_T10,36	259.46	259.58	259.79	259.61	0.05%	6.82	6.81	6.80	6.81	0.12%
S09_DN_45DEG_A389_T10,36	368.93	368.92	368.86	368.90	0.01%	11.09	11.11	11.11	11.10	0.09%
S09_DN_45DEG_A457_T10,36	433.58	433.66	432.85	433.36	0.09%	14.17	14.03	13.93	14.04	0.70%
S09_DN_45DEG_A594_T10,36	563.53	562.90	562.74	563.06	0.06%	21.43	21.45	21.46	21.45	0.07%

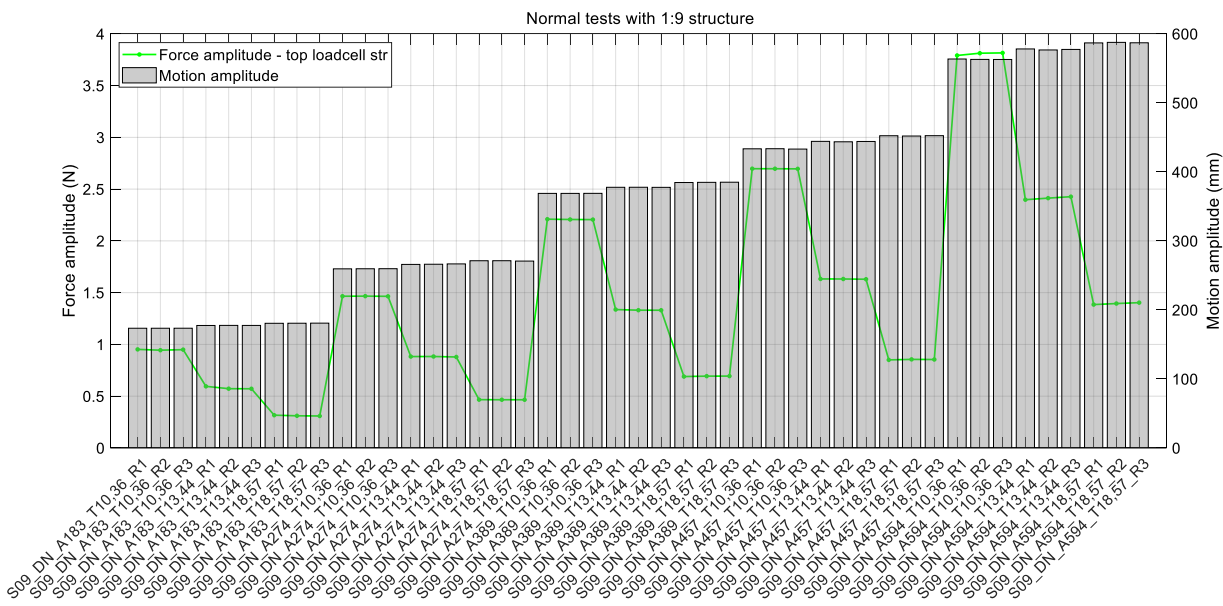


Figure A-6: Amplitudes of motion (bars) and load (blue curve) in each run – repeatability check for normal oscillations of the structure at 1:9 scale

A.3. Axial oscillations at 1:30 scale – 1st set of tests

Figure A-7 displays plots of both amplitude of motion and load as calculated through (3.1), the latter using the filtered signal. The amplitudes of motion are plotted as bars, while the load amplitude in a curve, for a better visualization of both parameters simultaneously. Each 3 consecutive points in the plot below represent the 3 runs of each case. One notices that the amplitude of motions does not vary significantly in each run. The amplitudes of load present slightly larger variation when compared to the motion, but still small enough to indicate repeatability of the test.

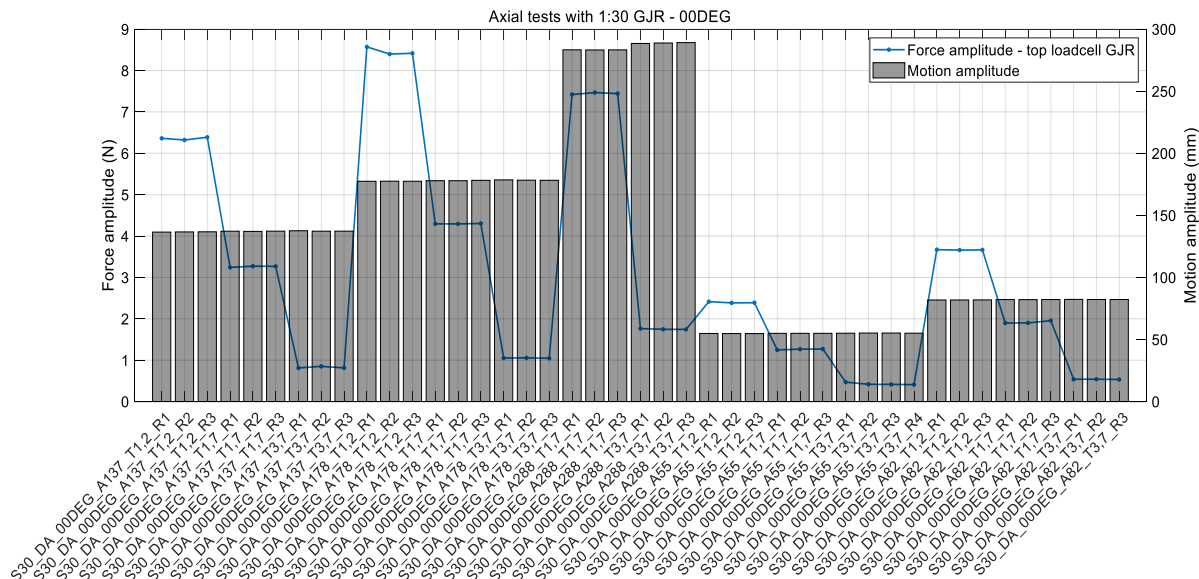


Figure A-7: Amplitudes of motion (bars) and load (blue curve) in each run – repeatability check for axial oscillations at 00DEG at 1:30 scale

Table A-5 presents the amplitudes of motion and load for each case, and the RMS error over the mean for each set of 3 runs. The error RMS over the mean value indicates a variation of less than 1% in all cases for the amplitude motion, while the variation in the load gets up to 5% with respect the mean value in some cases. The larger percentage, compared to what is observed for the motion, is due to the small mean value for the load, as seen below.

Table A-5: Repeatability check for 1:30 axial oscillations at 00DEG

CASE	AMPLITUDE OF MOTION					AMPLITUDE OF LOAD				
	R1 (mm)	R2 (mm)	R3 (mm)	MEAN (mm)	ERROR RMS %	R1 (N)	R2 (N)	R3 (N)	MEAN (N)	ERROR RMS %
S30_DA_00DEG_A55_T1,2	54.78	54.80	54.78	54.79	0.02%	2.41	2.39	2.39	2.40	0.49%
S30_DA_00DEG_A82_T1,2	81.89	81.88	81.83	81.87	0.03%	3.67	3.66	3.67	3.67	0.08%
S30_DA_00DEG_A137_T1,2	136.51	136.66	136.75	136.64	0.07%	6.36	6.32	6.39	6.36	0.43%
S30_DA_00DEG_A178_T1,2	177.47	177.57	177.28	177.44	0.07%	8.60	8.40	8.42	8.47	1.10%
S30_DA_00DEG_A288_T1,2	-	-	-	-	-	-	-	-	-	-
S30_DA_00DEG_A55_T1,7	55.04	55.09	54.98	55.04	0.08%	1.25	1.27	1.27	1.26	0.82%
S30_DA_00DEG_A82_T1,7	82.18	82.13	82.20	82.17	0.04%	1.90	1.90	1.97	1.92	1.66%
S30_DA_00DEG_A137_T1,7	137.27	136.93	137.27	137.16	0.12%	3.24	3.26	3.29	3.26	0.63%
S30_DA_00DEG_A178_T1,7	177.93	177.93	178.19	178.02	0.07%	4.32	4.34	4.30	4.32	0.40%
S30_DA_00DEG_A288_T1,7	283.35	283.23	283.31	283.30	0.02%	7.43	7.51	7.54	7.49	0.63%
S30_DA_00DEG_A55_T3,7	55.11	55.20	55.21	55.17	0.08%	0.41	0.42	0.42	0.41	0.86%
S30_DA_00DEG_A82_T3,7	82.47	82.26	82.34	82.36	0.10%	0.54	0.54	0.53	0.54	0.52%
S30_DA_00DEG_A137_T3,7	137.60	137.30	137.56	137.49	0.10%	0.81	0.85	0.82	0.83	2.11%
S30_DA_00DEG_A178_T3,7	178.57	178.37	178.46	178.47	0.05%	1.06	1.06	1.05	1.05	0.29%
S30_DA_00DEG_A288_T3,7	289.20	289.05	289.14	289.13	0.02%	1.77	1.74	1.75	1.75	0.55%

Similar analysis was performed for the axial oscillations with the model rotated by 45 degrees, showing similar behavior. The comparison of the load amplitudes between the model at 0 and at 45 degrees show similar values, indicating (without no advanced post processing) that the rotation does not affect the hydrodynamic loads on the gimbal.

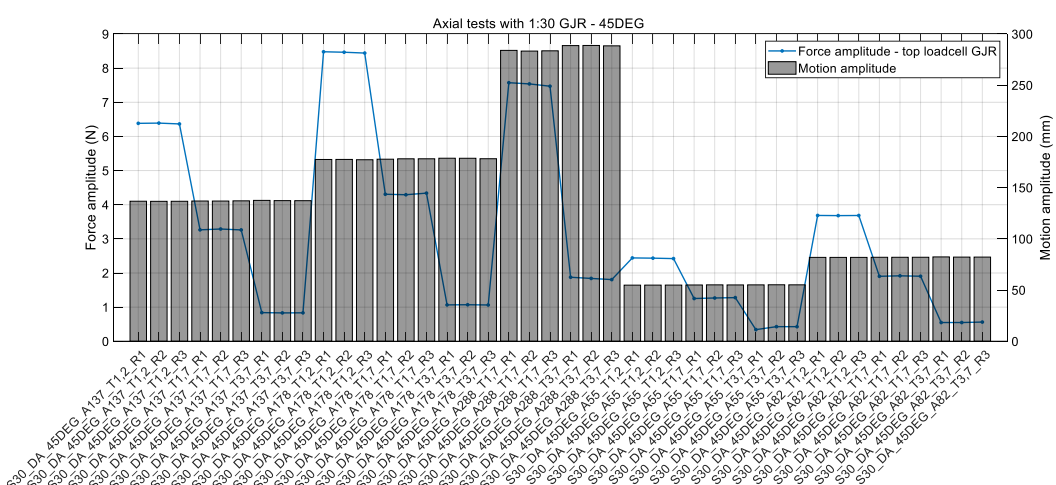


Figure A-8: Amplitudes of motion (bars) and load (blue curve) in each run – repeatability check for axial oscillations at 45DEG at 1:30 scale

Table A-6: Repeatability check for 1:30 axial oscillations at 45DEG

CASE	AMPLITUDE OF MOTION					AMPLITUDE OF LOAD				
	R1 (mm)	R2 (mm)	R3 (mm)	MEAN (mm)	ERROR RMS %	R1 (N)	R2 (N)	R3 (N)	MEAN (N)	ERROR RMS %
S30_DA_45DEG_A55_T1,2	54.78	54.81	54.85	54.81	0.06%	2.44	2.44	2.42	2.43	0.35%
S30_DA_45DEG_A82_T1,2	81.88	81.86	81.90	81.88	0.02%	3.68	3.68	3.71	3.69	0.31%
S30_DA_45DEG_A137_T1,2	136.72	136.63	136.67	136.67	0.03%	6.39	6.39	6.36	6.38	0.21%
S30_DA_45DEG_A178_T1,2	177.56	177.57	177.23	177.45	0.09%	8.47	8.46	8.44	8.46	0.14%
S30_DA_45DEG_A288_T1,2	-	-	-	-	-	-	-	-	-	-
S30_DA_45DEG_A55_T1,7	54.97	55.09	55.10	55.05	0.10%	1.26	1.27	1.28	1.27	0.65%
S30_DA_45DEG_A82_T1,7	82.21	82.19	82.03	82.15	0.10%	1.90	1.92	1.92	1.91	0.43%
S30_DA_45DEG_A137_T1,7	136.93	136.93	137.28	137.05	0.12%	3.27	3.28	3.26	3.27	0.30%
S30_DA_45DEG_A178_T1,7	177.84	178.17	178.19	178.07	0.09%	4.30	4.31	4.33	4.31	0.33%
S30_DA_45DEG_A288_T1,7	283.99	283.27	283.54	283.60	0.10%	7.66	7.59	7.56	7.60	0.56%
S30_DA_45DEG_A55_T3,7	55.10	55.16	55.08	55.11	0.07%	0.34	0.43	0.43	0.40	10.30%
S30_DA_45DEG_A82_T3,7	82.40	82.21	82.31	82.31	0.10%	0.55	0.55	0.56	0.55	1.14%
S30_DA_45DEG_A137_T3,7	137.55	137.32	137.55	137.47	0.08%	0.84	0.83	0.83	0.84	0.42%
S30_DA_45DEG_A178_T3,7	178.71	178.67	178.45	178.61	0.06%	1.07	1.07	1.07	1.07	0.26%
S30_DA_45DEG_A288_T3,7	289.20	289.05	288.43	288.89	0.12%	1.88	1.84	1.82	1.85	1.24%

Afterwards the tests with the gimbal model, the structure was oscillated alone to measure the loads acquired by the loadcells other than the desired, that is the hydrodynamic load on the gimbal. The ergodicity of this test was also verified in a similar manner, as illustrated by Figure A-9.

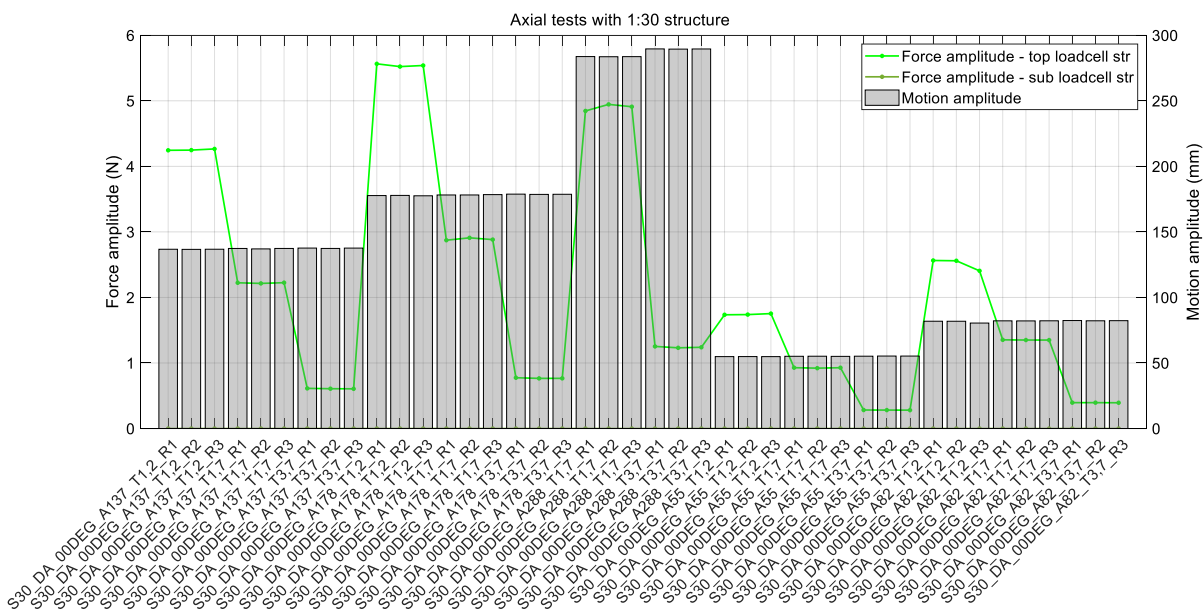


Figure A-9: Amplitudes of motion (bars) and load (blue curve) in each run – repeatability check for axial oscillations of the structure at 1:30 scale

A.4. Normal oscillations at 1:30 scale – 1st set of tests

Figures and tables summarize the repeatability check for the first set of normal oscillations at 1:30 set.

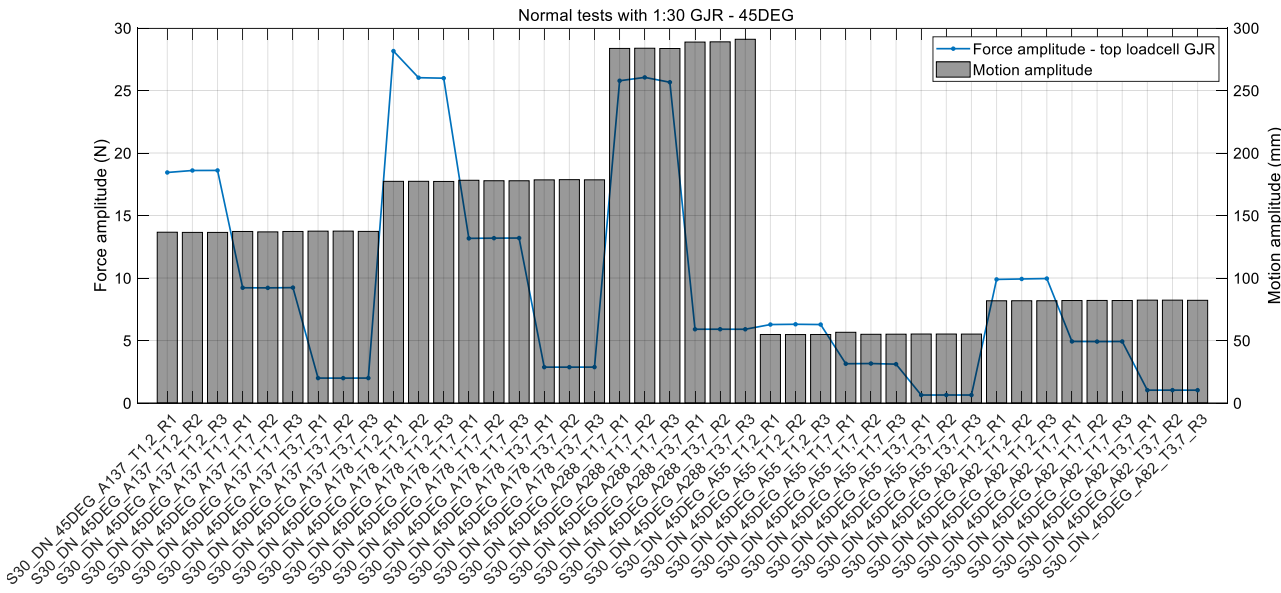


Figure A-10: Amplitudes of motion (bars) and load (blue curve) in each run – repeatability check for normal oscillations at 00DEG at 1:30 scale

Table A-7: Repeatability check for 1:30 normal oscillations at 00DEG

CASE	AMPLITUDE OF MOTION					AMPLITUDE OF LOAD				
	R1 (mm)	R2 (mm)	R3 (mm)	MEAN (mm)	ERROR RMS %	R1 (N)	R2 (N)	R3 (N)	MEAN (N)	ERROR RMS %
S30_DN_00DEG_A55_T1,2	55.06	55.00	55.07	55.05	0.06%	6.38	6.33	6.37	6.36	0.32%
S30_DN_00DEG_A82_T1,2	82.06	82.12	82.04	82.07	0.04%	9.94	10.00	9.98	9.97	0.26%
S30_DN_00DEG_A137_T1,2	137.15	137.02	137.02	137.06	0.04%	18.80	19.00	18.95	18.92	0.44%
S30_DN_00DEG_A178_T1,2	178.07	178.10	178.00	178.06	0.02%	26.38	26.98	26.75	26.70	0.94%
S30_DN_00DEG_A288_T1,2	-	-	-	-	-	-	-	-	-	-
S30_DN_00DEG_A55_T1,7	55.29	55.27	55.31	55.29	0.03%	3.20	3.21	3.18	3.20	0.40%
S30_DN_00DEG_A82_T1,7	82.46	82.28	82.30	82.34	0.10%	4.98	4.99	4.98	4.98	0.10%
S30_DN_00DEG_A137_T1,7	137.70	137.43	137.76	137.63	0.11%	9.65	9.57	9.56	9.59	0.40%
S30_DN_00DEG_A178_T1,7	178.59	178.57	178.98	178.71	0.11%	13.84	13.68	13.64	13.72	0.62%
S30_DN_00DEG_A288_T1,7	284.84	284.63	284.77	284.74	0.03%	26.95	27.14	27.09	27.06	0.29%
S30_DN_00DEG_A55_T3,7	55.44	55.42	55.44	55.44	0.02%	0.17	0.66	0.65	0.50	45.83%
S30_DN_00DEG_A82_T3,7	82.63	82.54	82.52	82.56	0.06%	1.05	1.06	1.06	1.06	0.42%
S30_DN_00DEG_A137_T3,7	137.87	137.74	137.78	137.80	0.04%	2.09	2.06	2.08	2.08	0.58%
S30_DN_00DEG_A178_T3,7	179.28	179.05	179.13	179.15	0.05%	3.02	3.02	3.01	3.01	0.16%
S30_DN_00DEG_A288_T3,7	289.98	290.17	289.99	290.05	0.03%	6.22	6.22	6.23	6.22	0.09%

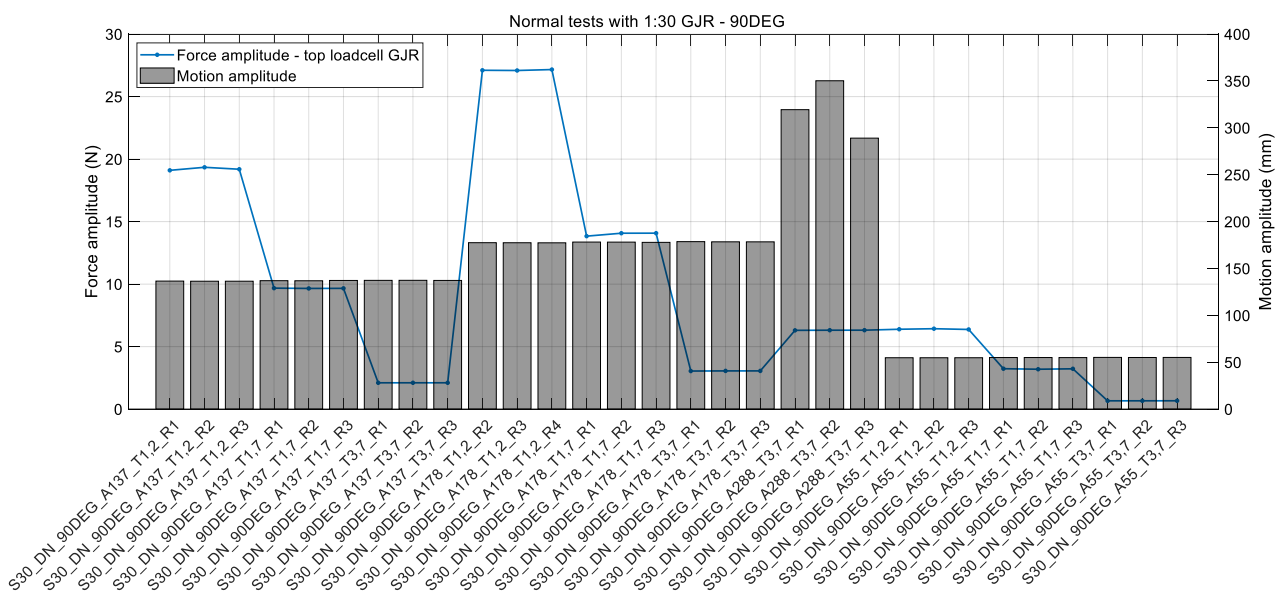


Figure A-11: Amplitudes of motion (bars) and load (blue curve) in each run – repeatability check for normal oscillations at 45DEG at 1:30 scale

Table A-8: Repeatability check for 1:30 normal oscillations at 45DEG

CASE	AMPLITUDE OF MOTION					AMPLITUDE OF LOAD				
	R1 (mm)	R2 (mm)	R3 (mm)	MEAN (mm)	ERROR RMS %	R1 (N)	R2 (N)	R3 (N)	MEAN (N)	ERROR RMS %
S30_DN_45DEG_A55_T1,2	54.83	54.78	54.83	54.82	0.05%	6.28	6.30	6.28	6.29	0.16%
S30_DN_45DEG_A82_T1,2	81.79	81.82	81.82	81.81	0.01%	9.89	9.92	9.96	9.92	0.28%
S30_DN_45DEG_A137_T1,2	136.64	136.49	136.49	136.54	0.05%	18.44	18.60	18.61	18.55	0.41%
S30_DN_45DEG_A178_T1,2	177.34	177.36	177.25	177.32	0.03%	28.16	26.03	25.98	26.72	3.80%
S30_DN_45DEG_A288_T1,2	-	-	-	-	-	-	-	-	-	-
S30_DN_45DEG_A55_T1,7	56.59	54.99	55.06	55.55	1.33%	3.14	3.16	3.11	3.14	0.65%
S30_DN_45DEG_A82_T1,7	81.99	82.06	82.00	82.02	0.04%	4.93	4.92	4.92	4.92	0.09%
S30_DN_45DEG_A137_T1,7	137.23	136.91	137.24	137.13	0.11%	9.22	9.21	9.23	9.22	0.09%
S30_DN_45DEG_A178_T1,7	178.19	177.82	177.80	177.94	0.10%	13.17	13.19	13.20	13.19	0.08%
S30_DN_45DEG_A288_T1,7	283.66	283.81	283.60	283.69	0.03%	25.78	26.05	25.66	25.83	0.63%
S30_DN_45DEG_A55_T3,7	55.20	55.19	55.15	55.18	0.04%	0.64	0.64	0.64	0.64	0.22%
S30_DN_45DEG_A82_T3,7	82.31	82.31	82.17	82.26	0.08%	1.03	1.03	1.03	1.03	0.11%
S30_DN_45DEG_A137_T3,7	137.50	137.53	137.30	137.44	0.07%	2.00	1.99	2.00	1.99	0.10%
S30_DN_45DEG_A178_T3,7	178.52	178.68	178.55	178.58	0.04%	2.87	2.87	2.87	2.87	0.08%
S30_DN_45DEG_A288_T3,7	288.75	288.92	290.98	289.55	0.35%	5.90	5.90	5.90	5.90	0.03%

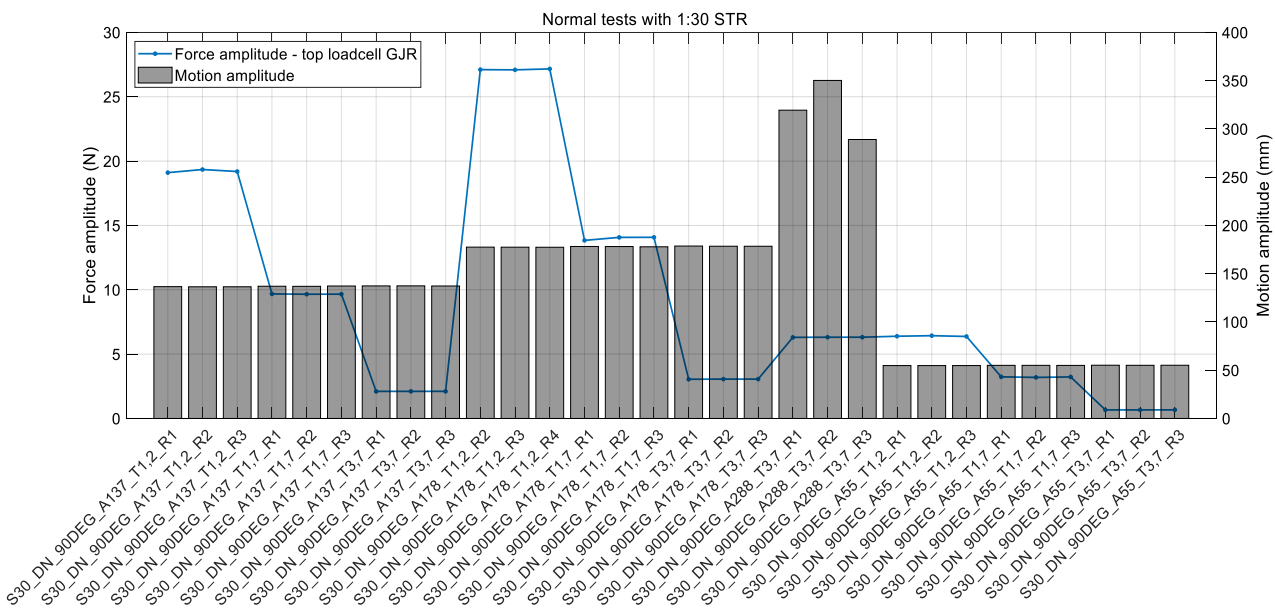


Figure A-12: Amplitudes of motion (bars) and load (blue curve) in each run – repeatability check for normal oscillations at 90DEG at 1:30 scale

Table A-9: Repeatability check for 1:30 normal oscillations at 90DEG

CASE	AMPLITUDE OF MOTION					AMPLITUDE OF LOAD				
	R1 (mm)	R2 (mm)	R3 (mm)	MEAN (mm)	ERROR RMS %	R1 (N)	R2 (N)	R3 (N)	MEAN (N)	ERROR RMS %
S30_DN_90DEG_A55_T1,2	54.83	54.82	54.83	54.83	0.01%	6.39	6.43	6.37	6.40	0.40%
S30_DN_90DEG_A82_T1,2	-	-	-	-	-	-	-	-	-	-
S30_DN_90DEG_A137_T1,2	136.59	136.44	136.46	136.50	0.05%	19.10	19.35	19.19	19.21	0.52%
S30_DN_90DEG_A178_T1,2	177.54	177.48	177.41	177.47	0.03%	27.11	27.09	27.17	27.12	0.12%
S30_DN_90DEG_A288_T1,2	-	-	-	-	-	-	-	-	-	-
S30_DN_90DEG_A55_T1,7	55.04	55.06	54.99	55.03	0.05%	3.24	3.19	3.23	3.22	0.58%
S30_DN_90DEG_A82_T1,7	82.20	82.04	82.01	82.08	0.10%	5.03	5.04	5.03	5.04	0.09%
S30_DN_90DEG_A137_T1,7	137.01	136.93	137.27	137.07	0.10%	9.68	9.66	9.66	9.67	0.10%
S30_DN_90DEG_A178_T1,7	178.20	178.15	177.88	178.08	0.08%	13.84	14.07	14.08	14.00	0.80%
S30_DN_90DEG_A288_T1,7	-	-	-	-	-	-	-	-	-	-
S30_DN_90DEG_A55_T3,7	55.18	55.09	55.15	55.14	0.07%	0.67	0.67	0.67	0.67	0.21%
S30_DN_90DEG_A82_T3,7	82.33	82.23	82.18	82.25	0.07%	1.07	1.07	1.07	1.07	0.03%
S30_DN_90DEG_A137_T3,7	137.35	137.41	137.28	137.35	0.04%	2.11	2.11	2.11	2.11	0.05%
S30_DN_90DEG_A178_T3,7	178.65	178.46	178.44	178.52	0.05%	3.05	3.06	3.06	3.06	0.17%
S30_DN_90DEG_A288_T3,7	319.43	350.24	289.06	319.58	7.82%	6.30	6.31	6.32	6.31	0.09%

Afterwards the tests with the gimbal model, the structure was oscillated alone to measure the loads acquired by the loadcells other than the desired, that is the hydrodynamic load on the gimbal. The ergodicity of this test was also verified in a similar manner, as illustrated by Figure A-13.

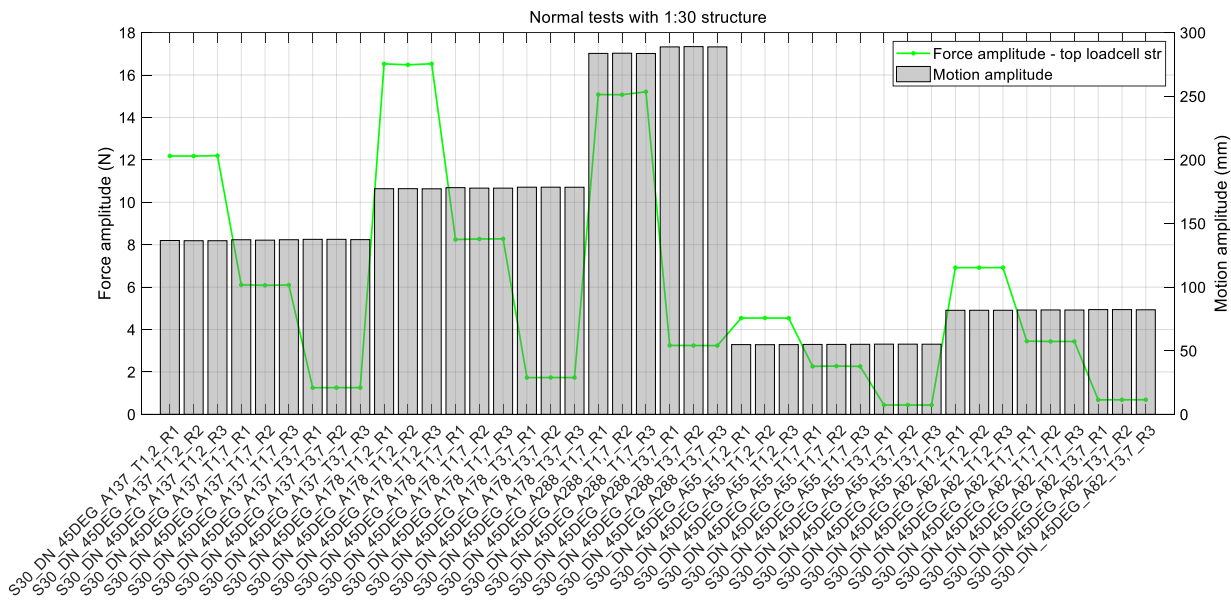


Figure A-13: Amplitudes of motion (bars) and load (blue curve) in each run – repeatability check for normal oscillations of the structure at 1:30 scale

A.5. Axial oscillations at 1:30 scale – 2nd set of tests

A second set of tests was carried out at 1:30 scale for the 00DEG conditions only. The plots and tables below present the repeatability analysis for this set.

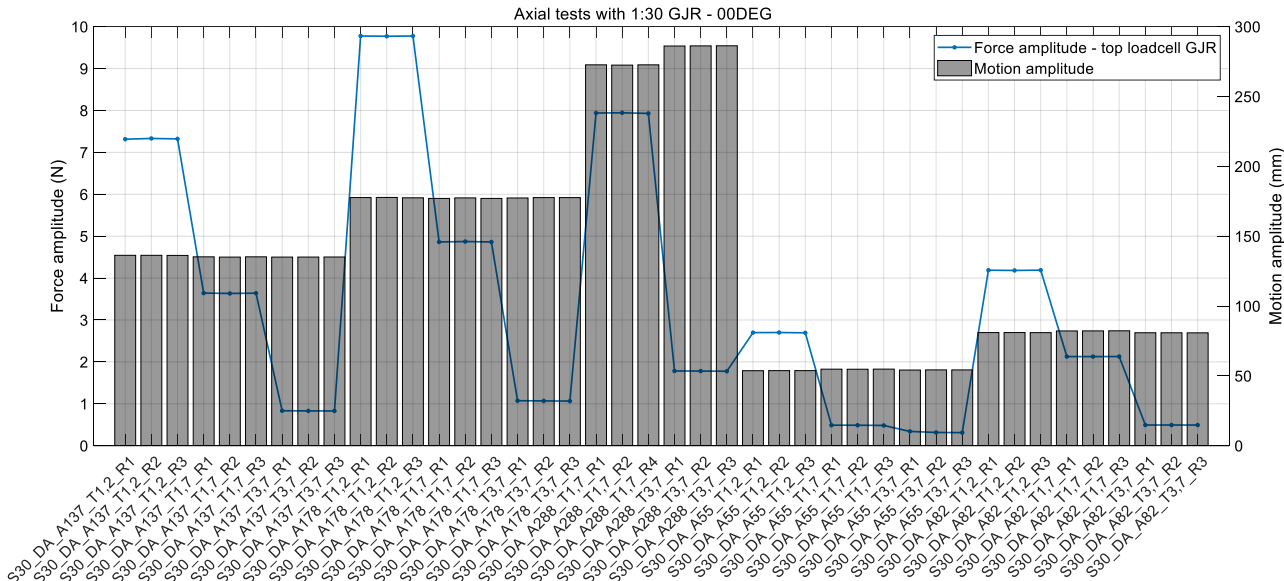


Figure A-14: Amplitudes of motion (bars) and load (blue curve) in each run – repeatability check for second set of axial oscillations of the GJR at 1:30 scale

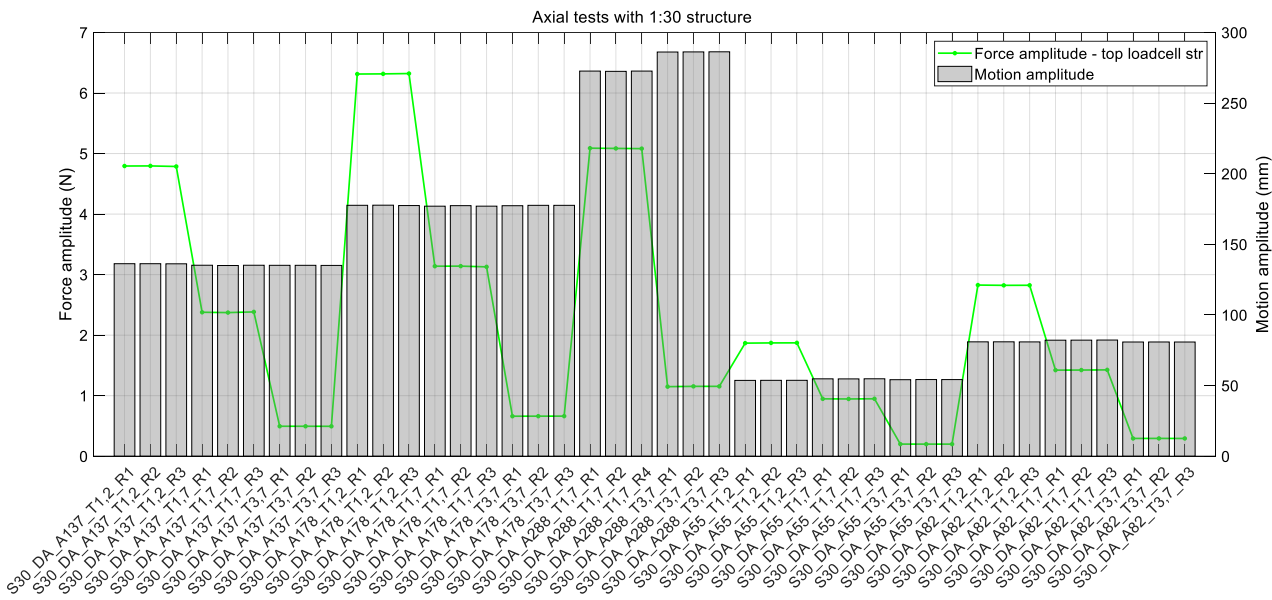


Figure A-15: Amplitudes of motion (bars) and load (blue curve) in each run – repeatability check for second set of axial oscillations of the structure at 1:30 scale

Table A-10: Repeatability check for second set of 1:30 axial oscillations at 00DEG

CASE	AMPLITUDE OF MOTION					AMPLITUDE OF LOAD				
	R1 (mm)	R2 (mm)	R3 (mm)	MEAN (mm)	ERROR RMS %	R1 (N)	R2 (N)	R3 (N)	MEAN (N)	ERROR RMS %
S30_DA_00DEG_A55_T1,2	53.69	53.74	53.74	53.73	0.05%	2.70	2.70	2.69	2.70	0.11%
S30_DA_00DEG_A82_T1,2	80.98	81.00	80.94	80.97	0.03%	4.19	4.18	4.19	4.19	0.07%
S30_DA_00DEG_A137_T1,2	136.30	136.29	136.23	136.27	0.02%	7.31	7.33	7.32	7.32	0.10%
S30_DA_00DEG_A178_T1,2	135.03	135.05	135.10	135.06	0.02%	0.83	0.83	0.83	0.83	0.22%
S30_DA_00DEG_A288_T1,2	-	-	-	-	-	-	-	-	-	-
S30_DA_00DEG_A55_T1,7	54.80	54.75	54.83	54.79	0.05%	0.49	0.49	0.48	0.49	0.59%
S30_DA_00DEG_A82_T1,7	82.16	82.19	82.25	82.20	0.05%	2.13	2.13	2.13	2.13	0.04%
S30_DA_00DEG_A137_T1,7	135.21	135.02	135.21	135.15	0.06%	3.64	3.63	3.64	3.64	0.10%
S30_DA_00DEG_A178_T1,7	177.02	177.40	177.03	177.15	0.10%	4.86	4.87	4.86	4.87	0.10%
S30_DA_00DEG_A288_T1,7	272.67	272.47	272.66	272.60	0.03%	7.94	7.94	7.93	7.94	0.08%
S30_DA_00DEG_A55_T3,7	54.17	54.27	54.25	54.23	0.09%	0.34	0.32	0.31	0.32	3.96%
S30_DA_00DEG_A82_T3,7	80.87	80.84	80.80	80.83	0.03%	0.49	0.49	0.49	0.49	0.08%
S30_DA_00DEG_A137_T3,7	135.03	135.05	135.10	135.06	0.02%	0.83	0.83	0.83	0.83	0.22%
S30_DA_00DEG_A178_T3,7	177.35	177.61	177.61	177.52	0.07%	1.07	1.07	1.06	1.07	0.33%
S30_DA_00DEG_A288_T3,7	286.14	286.23	286.30	286.22	0.02%	1.78	1.78	1.78	1.78	0.16%

In the second set of tests, given the observation that the angle of the model would not affect the hydrodynamic loads on the GJR and only the 00DEG cases were tested, it was decided to increase the number of oscillation conditions to explore other combinations of amplitudes and periods (KC and Reynolds). Each additional case was run thrice, as the original ones.

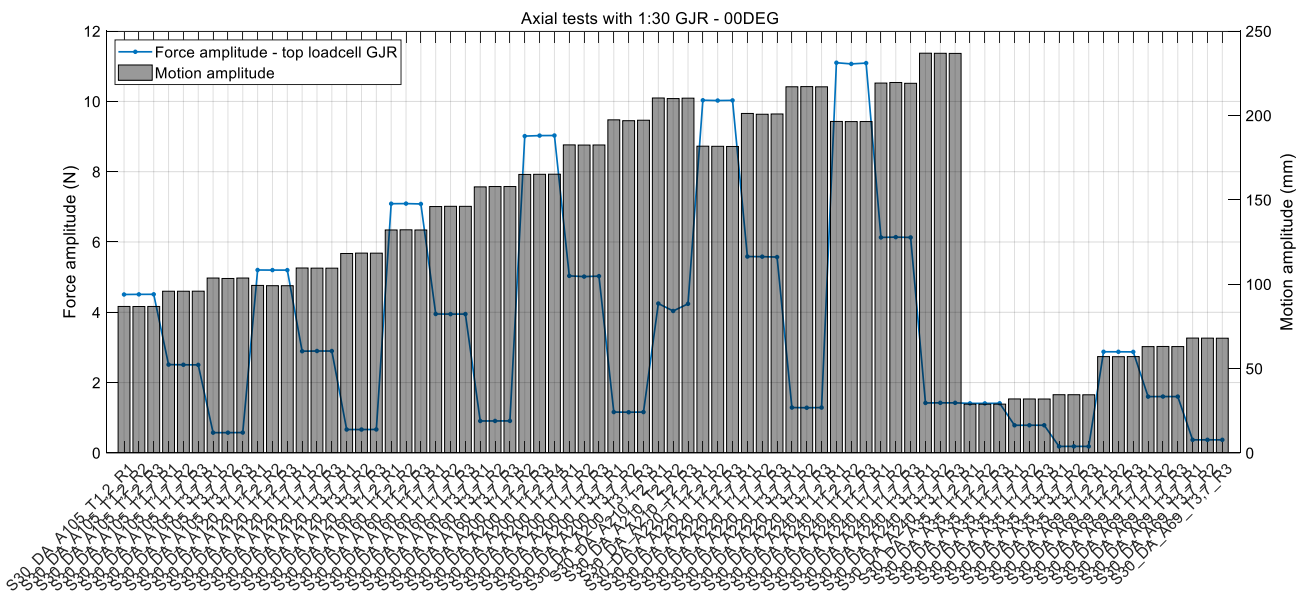


Figure A-16: Amplitudes of motion (bars) and load (blue curve) in each run – repeatability check for second set of axial oscillations of the GJR at 1:30 scale for additional cases

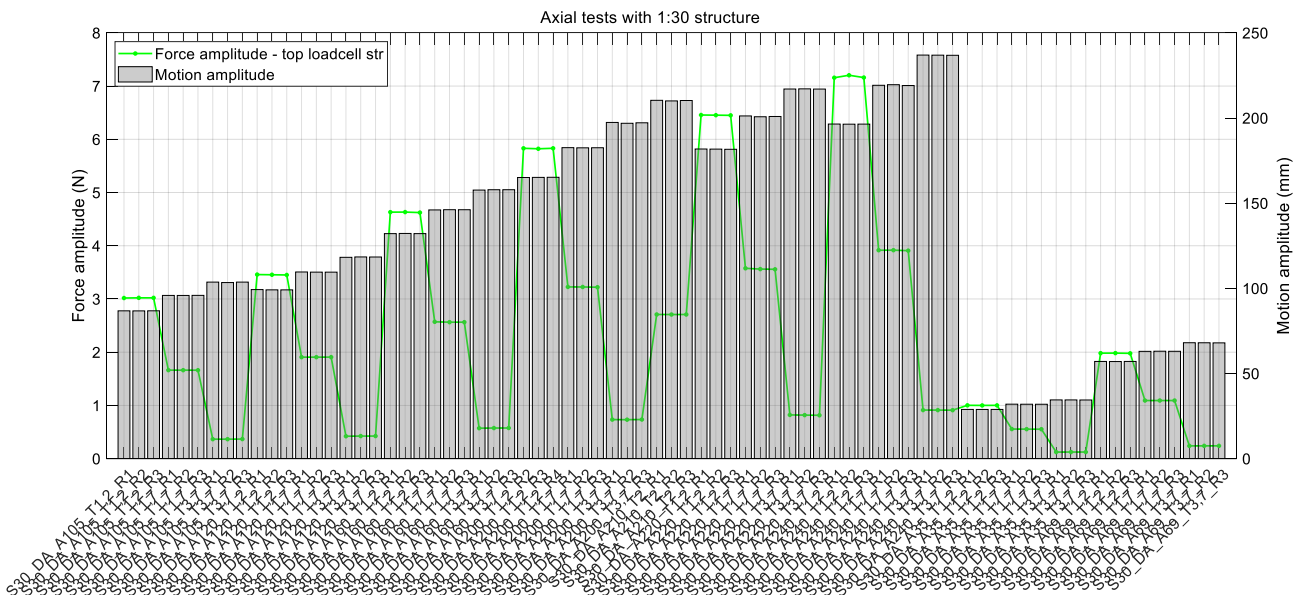


Figure A-17: Amplitudes of motion (bars) and load (blue curve) in each run – repeatability check for second set of axial oscillations of the structure at 1:30 scale for additional cases

A.6. Normal oscillations at 1:30 scale – 2nd set of tests

As in the axial cases, a set of additional oscillation conditions were tested, as illustrated by the repeatability check in Figure A-18 for the test with the model and in Figure A-19 for the structure alone and summarized in Table A-11.

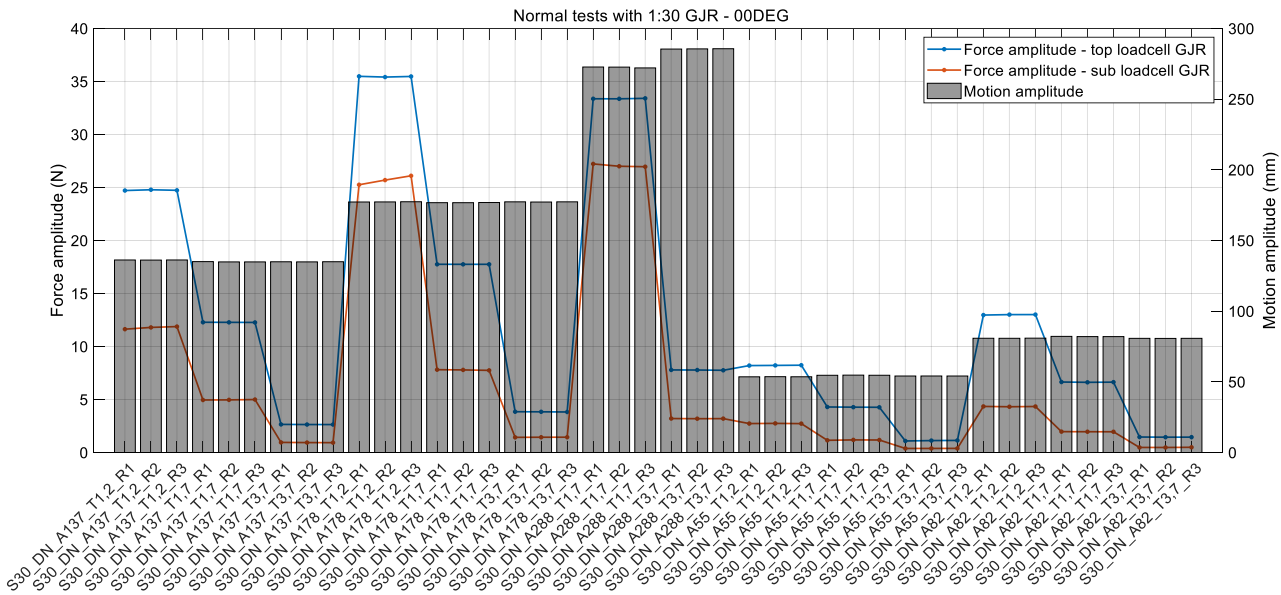


Figure A-18: Amplitudes of motion (bars) and load (blue curve) in each run – repeatability check for second set of normal oscillations of the GJR at 1:30 scale

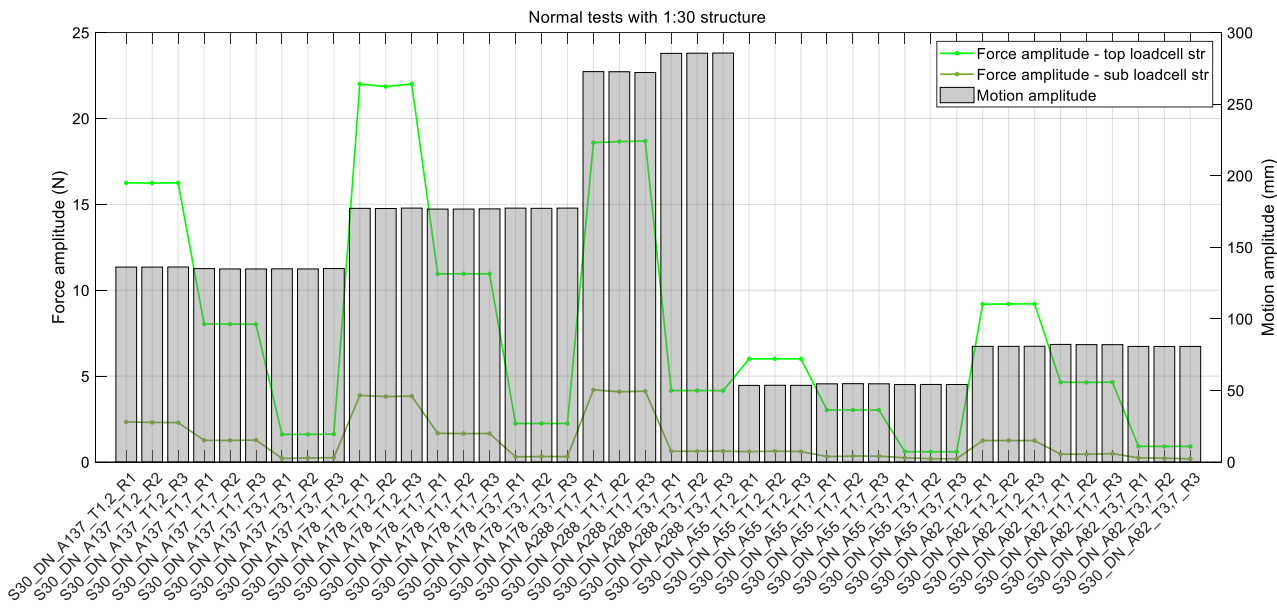


Figure A-19: Amplitudes of motion (bars) and load (blue curve) in each run – repeatability check for second set of normal oscillations of the structure at 1:30 scale

Table A-11: Repeatability check for second set of 1:30 axial oscillations at 00DEG

CASE	AMPLITUDE OF MOTION					AMPLITUDE OF LOAD				
	R1 (mm)	R2 (mm)	R3 (mm)	MEAN (mm)	ERROR RMS %	R1 (N)	R2 (N)	R3 (N)	MEAN (N)	ERROR RMS %
S30_DN_00DEG_A55_T1,2	53.55	53.64	53.58	53.59	0.07%	8.20	8.22	8.23	8.22	0.17%
S30_DN_00DEG_A82_T1,2	80.82	80.79	80.89	80.84	0.05%	12.96	13.01	13.01	12.99	0.16%
S30_DN_00DEG_A137_T1,2	136.21	136.13	136.21	136.18	0.03%	24.71	24.79	24.73	24.74	0.13%
S30_DN_00DEG_A178_T1,2	177.23	177.28	177.40	177.31	0.04%	35.49	35.41	35.47	35.46	0.09%
S30_DN_00DEG_A288_T1,2	-	-	-	-	-	-	-	-	-	-
S30_DN_00DEG_A55_T1,7	54.63	54.74	54.65	54.67	0.09%	4.29	4.28	4.26	4.28	0.28%
S30_DN_00DEG_A82_T1,7	82.15	82.00	81.99	82.05	0.09%	6.65	6.62	6.64	6.63	0.18%
S30_DN_00DEG_A137_T1,7	135.05	134.84	134.84	134.91	0.07%	12.28	12.28	12.27	12.28	0.05%
S30_DN_00DEG_A178_T1,7	176.74	176.74	176.86	176.78	0.03%	17.75	17.75	17.75	17.75	0.01%
S30_DN_00DEG_A288_T1,7	272.73	272.66	272.09	272.49	0.11%	33.37	33.36	33.41	33.38	0.06%
S30_DN_00DEG_A55_T3,7	54.12	54.13	54.11	54.12	0.01%	1.09	1.12	1.14	1.12	1.99%
S30_DN_00DEG_A82_T3,7	80.76	80.71	80.76	80.74	0.03%	1.46	1.44	1.45	1.45	0.46%
S30_DN_00DEG_A137_T3,7	134.94	134.86	134.97	134.92	0.03%	2.65	2.64	2.64	2.64	0.23%
S30_DN_00DEG_A178_T3,7	177.34	177.21	177.34	177.30	0.03%	3.85	3.84	3.82	3.84	0.26%
S30_DN_00DEG_A288_T3,7	285.43	285.55	285.67	285.55	0.03%	7.79	7.78	7.76	7.77	0.18%

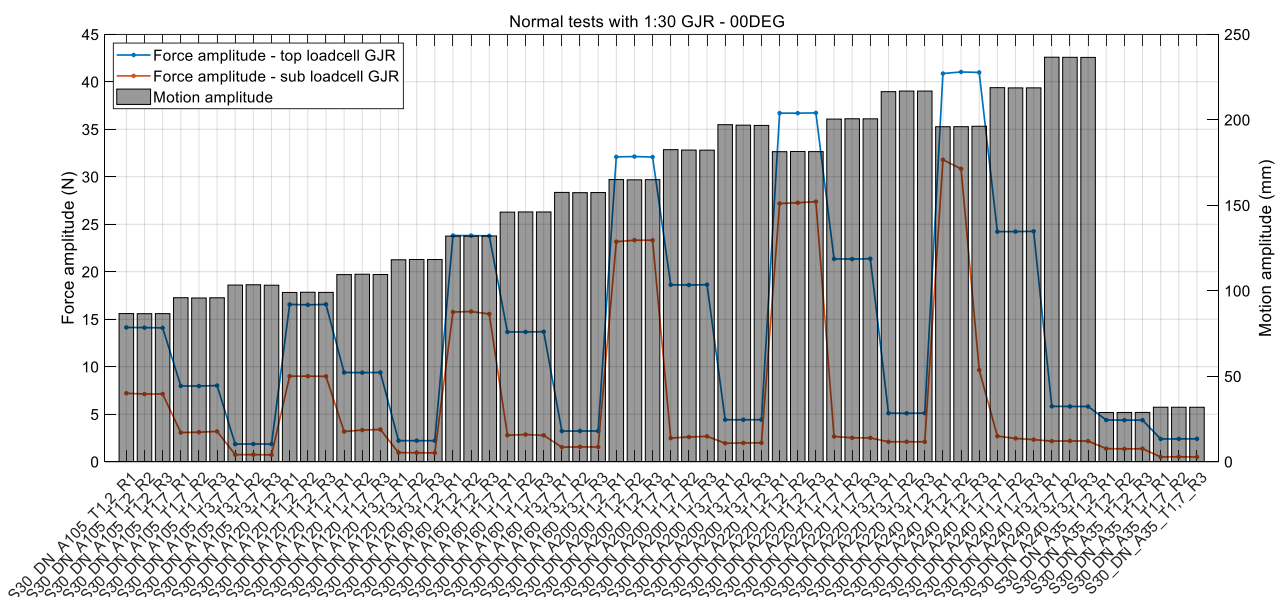


Figure A-20: Amplitudes of motion (bars) and load (blue curve) in each run – repeatability check for second set of axial oscillations of the GJR at 1:30 scale for additional cases

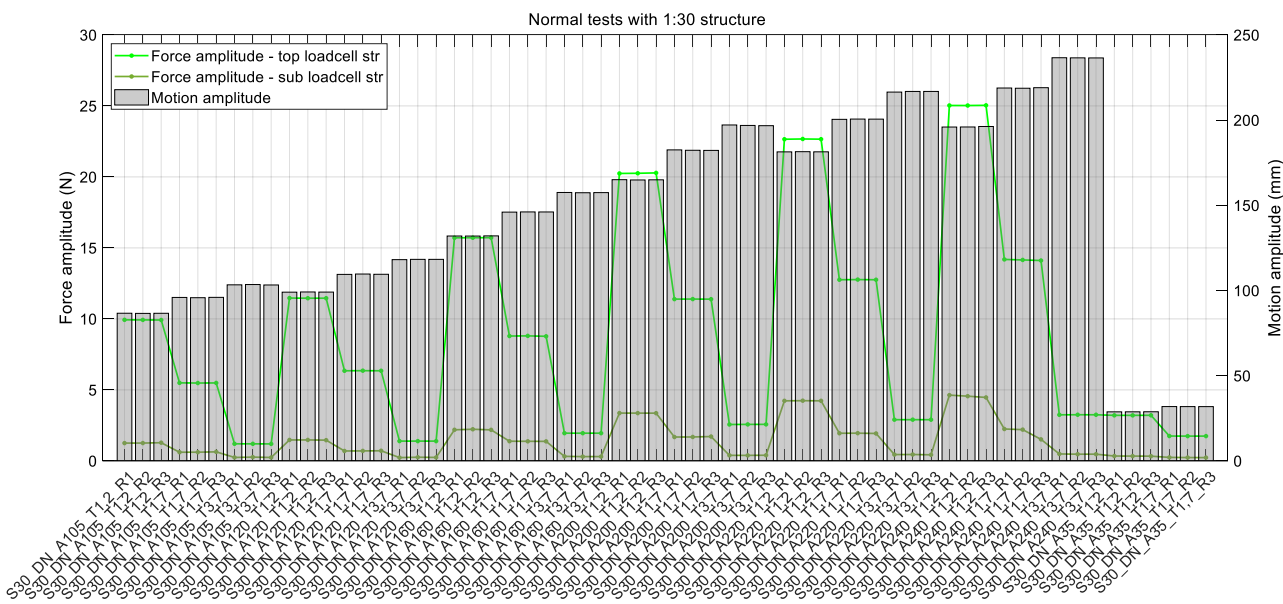


Figure A-21: Amplitudes of motion (bars) and load (blue curve) in each run – repeatability check for second set of axial oscillations of the structure at 1:30 scale for the additional cases

Table A-12: Repeatability check for additional cases on set #2 of 1:30 normal oscillations at 00DEG

CASE	AMPLITUDE OF MOTION					AMPLITUDE OF LOAD				
	R1 (mm)	R2 (mm)	R3 (mm)	MEAN (mm)	ERROR RMS %	R1 (N)	R2 (N)	R3 (N)	MEAN (N)	ERROR RMS %
S30_DN_00DEG_A105_T1,2	86.65	86.57	86.61	86.61	0.04%	14.13	14.12	14.09	14.11	0.13%
S30_DN_00DEG_A105_T1,7	95.91	95.76	95.87	95.85	0.07%	7.97	7.96	8.02	7.98	0.29%
S30_DN_00DEG_A105_T3,7	103.32	103.49	103.23	103.35	0.10%	1.85	1.86	1.85	1.86	0.28%
S30_DN_00DEG_A120_T1,2	99.00	99.12	99.04	99.05	0.05%	16.56	16.51	16.57	16.55	0.14%
S30_DN_00DEG_A120_T1,7	109.44	109.65	109.50	109.53	0.08%	9.39	9.38	9.40	9.39	0.09%
S30_DN_00DEG_A120_T3,7	118.10	118.27	118.26	118.21	0.06%	2.21	2.22	2.21	2.21	0.11%
S30_DN_00DEG_A160_T1,2	131.97	131.95	132.05	131.99	0.03%	23.81	23.81	23.78	23.80	0.05%
S30_DN_00DEG_A160_T1,7	145.98	146.09	146.07	146.04	0.03%	13.66	13.66	13.68	13.67	0.07%
S30_DN_00DEG_A160_T3,7	157.51	157.36	157.43	157.43	0.04%	3.22	3.23	3.23	3.23	0.09%
S30_DN_00DEG_A200_T1,2	165.02	164.87	164.96	164.95	0.04%	32.09	32.13	32.08	32.10	0.06%
S30_DN_00DEG_A200_T1,7	182.50	182.28	182.22	182.34	0.07%	18.62	18.60	18.64	18.62	0.08%
S30_DN_00DEG_A200_T3,7	197.12	196.84	196.69	196.88	0.09%	4.42	4.42	4.42	4.42	0.03%
S30_DN_00DEG_A220_T1,2	181.33	181.43	181.37	181.38	0.02%	36.70	36.70	36.72	36.71	0.04%
S30_DN_00DEG_A220_T1,7	200.40	200.59	200.55	200.51	0.04%	21.35	21.33	21.37	21.35	0.07%
S30_DN_00DEG_A220_T3,7	216.43	216.79	216.79	216.67	0.08%	5.11	5.09	5.11	5.10	0.15%
S30_DN_00DEG_A240_T1,2	195.93	195.94	196.22	196.03	0.07%	40.87	41.03	40.98	40.96	0.17%
S30_DN_00DEG_A240_T1,7	218.78	218.65	218.66	218.70	0.03%	24.22	24.23	24.25	24.23	0.06%
S30_DN_00DEG_A240_T3,7	236.59	236.53	236.48	236.54	0.02%	5.83	5.81	5.81	5.82	0.13%